cipitation assay. As shown in Fig. 8C, double replacing both Lys^{97} and Arg^{98} with Ala (9798A) completely abrogated the interaction with Caprin-1. The importance of these two amino acids in the interaction with Caprin-1 was also confirmed by GST pulldown assay (Fig. 8D). These results indicate that Lys^{97} and Arg^{98} in the JEV core protein are crucial for the interaction with Caprin-1. Since G3BP has been reported to be one of the key molecules for SG formation and interacts with several SG component molecules including Caprin-1 and USP10 (28, 29), interactions of the core protein with SG components were examined by immunoprecipitation assay. The wild-type but not mutant 9798A core protein was associated with G3BP1 and USP10 (Fig. 8E). In addition, the knockdown of Caprin-1 weakened the interactions of core protein with G3BP1 or USP10 (Fig. 8F). These findings indicate that JEV core protein associates with several SG component molecules, such as G3BP1 and USP10, through the interaction with Caprin-1. Next, the role of the interaction between JEV core protein and Caprin-1 in the suppression of SG formation was examined by immunofluorescence analysis. Although the expression of the wild-type JEV core protein suppressed the SG formation induced by sodium arsenite treatment, as shown above, expression of the 9798A mutant did not (Fig. 8G), suggesting that the interaction of JEV core protein with Caprin-1 through Lys^{97} and Arg^{98} plays a crucial role in the inhibition of SG formation.

Interaction of the JEV core protein with Caprin-1 plays crucial roles not only in viral propagation *in vitro* but also in the pathogenesis in mice through the suppression of SG formation. To further examine the biological significance of the interaction between the JEV core protein and Caprin-1 in viral replication, we generated a mutant infectious cDNA clone (pMWJEAT/9798AA) of JEV encoding a mutant core protein deficient in the binding to Caprin-1 based on pMWJEAT. First, the cellular localization of the core protein in the 9798A mutant JEV-infected cells was examined by immunofluorescence analysis. The 9798A mutant core protein, as well as the wild-type core protein, was localized in the nucleus and the perinuclear region (Fig. 9A). However, the 9798A mutant core protein was not colocalized with Caprin-1, in contrast to the wild-type core protein. The sizes of infectious foci in Vero cells infected with the 9798A mutant were significantly smaller than those infected with the wild-type JEV (Fig. 9B). Furthermore, the infectious titers in C6/36 and Vero cells infected with the 9798A mutant were 6.1- and 12.6-fold lower than those infected with wild-type JEV at 48 h postinfection, respectively (Fig. 9C), suggesting that interaction of the JEV core protein with Caprin-1 plays crucial roles in the propagation of JEV in both insect and mammalian cells. Cells infected with the 9798A mutant induced SGs containing both G3BP and Caprin-1, in contrast to the accumulation of G3BP in the perinuclear region observed in those infected with the wild-type JEV (Fig. 9D). The numbers of foci in cells infected with the 9798A mutant were higher than those in cells infected with the wild-type JEV (Fig. 9E), indicating that the interaction of the JEV core protein with Caprin-1 is crucial for the suppression of SG formation. Finally, we examined the biological relevance of the interaction of JEV core protein with Caprin-1 in viral replication *in vivo*. Infectious particles were recovered from the cerebrums of ICR mice inoculated with wild-type JEV but not from those inoculated with the 9798A mutant (Fig. 9F). In addition, all 10 mice had died by 12 days postinoculation with the wild-type JEV, while only 1 mouse had died at day 10 postinoculation with the 9798A mutant (Fig. 9G). Collectively, these results suggest that the interaction of JEV core protein with Caprin-1 plays crucial roles not only in viral replication *in vitro* but also in pathogenesis in mice through the suppression of SG formation.

DISCUSSION

Viruses are obligatory intracellular parasites, and their life cycles rely on host cellular functions. Many viruses have evolved to inhibit SG formation and thereby evade the host translation shutoff mechanism and facilitate viral replication (6, 30), while some viruses co-opt molecules regulating SG formation for viral replication (11, 31). The vaccinia virus subverts SG components to generate aggregates containing G3BP, Caprin-1, eIF4G, eIF4E, and mRNA of the virus, but not of the host, in order to stimulate viral translation (11). Replication, translation, and assembly of transmissible gastroenteritis coronavirus, a member of the *Coronaviridae* family, are regulated by the interaction of polypyrimidine tract-binding protein and TIA-1 with viral RNA (31). HIV-1 utilizes Staufen1, which is a principal component of SG, in the viral RNA selection to form ribonucleoproteins (RNPs) through interaction with Gag protein, instead of SG translation silencing (8). In the case of flaviviruses, TIA-1 and TIAR bind to the 3′ untranslated region (UTR) of the negative-stranded RNA of WNV to facilitate viral replication (16), and G3BP1, Caprin-1, and USP10 interact with DENV RNA, although the biological significance of these interactions remains unknown (26). In this study, we have shown that JEV infection suppresses SG formation by the recruitment of several effector molecules promoting SG assembly, including G3BP and USP10, to the perinuclear region through the interaction of JEV core protein with Caprin-1. Furthermore, a mutant JEV carrying a core protein incapable of binding to

FIG 8 Lys^{97} and Arg^{98} in the JEV core protein are crucial residues for the interaction with Caprin-1. (A) Putative structural model of the core protein homodimer of JEV deduced from that of DENV obtained from the Protein Data Bank (accession number 1R6R) by using PyMOL software. The two α helices (α1 and α4) are indicated. (B) FLAG-Core mutants in which the hydrophobic amino acid residues in the α1 helix (Mα1) or α4 helix (Mα4) were replaced with alanine were coexpressed with HA-Caprin-1 in 293T cells, immunoprecipitated (IP) with anti-HA antibody, and examined by immunoblotting (IB) with anti-HA or anti-FLAG antibody. (C) FLAG-Core mutants in which the Met^{78}, Lys^{79}, Lys^{85}, Arg^{86}, Ile^{92}, and Asp^{93} (7893A) or Lys^{97} and Arg^{98} (9798A) in the α4 helix domain were replaced with alanine were coexpressed with HA-Caprin-1 in 293T cells and examined as described in panel B. (D) The His-tagged JEV core protein (WT or 9798A) was incubated with GST-fused Caprin-1 for 2 h at 4°C, and the precipitates obtained by GST pulldown assay were subjected to immunoblotting with anti-His antibody. (E) FLAG-Core (WT or 9798A) was coexpressed with HA-G3BP1 or HA-USP10 in 293T cells, immunoprecipitated with anti-HA antibody, and immunoblotted with anti-HA and anti-FLAG antibodies. (F) FLAG-JEV Core was coexpressed with HA-G3BP1 or HA-USP10 in 293T cells transfected with either siCaprin-1 or siNC at 72 h posttransfection, immunoprecipitated with anti-FLAG antibody, and immunoblotted with anti-HA and anti-FLAG antibodies. The cell lysates were also subjected to immunoblotting with anti-Caprin-1 and anti-β-actin antibodies to evaluate the knockdown efficiency of Caprin-1. (G) The cellular localizations of G3BP and FLAG-Core (WT or 9798A) were determined at 24 h posttransfection after treatment with 1.0 mM sodium arsenite for 30 min at 37°C by immunofluorescence analysis with mouse anti-G3BP MAb and rabbit anti-FLAG PAb, followed by AF488-conjugated anti-mouse IgG and AF594-conjugated anti-rabbit IgG, respectively. Cell nuclei were stained with DAPI (blue).

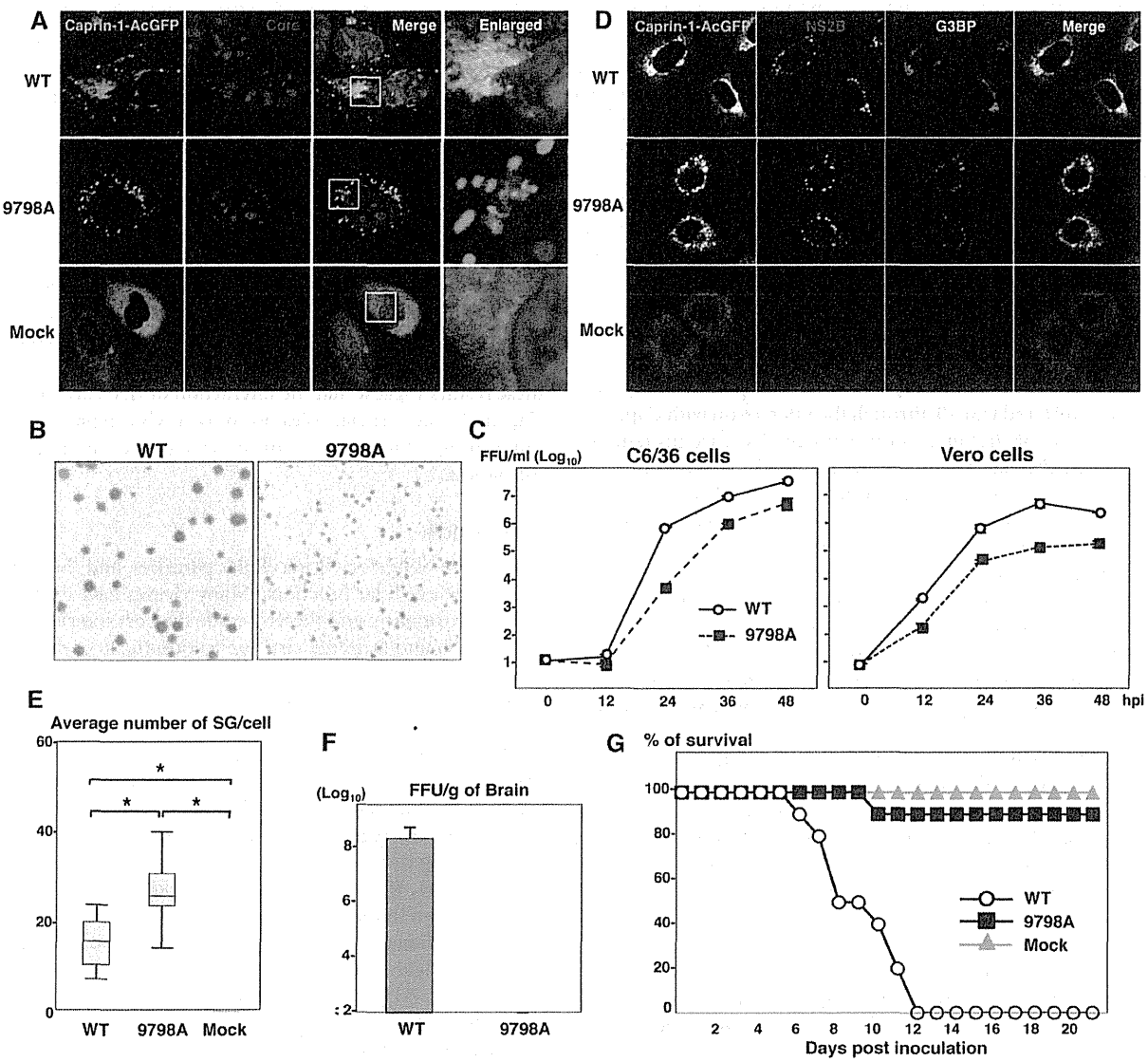

FIG 9 Interaction of JEV core protein with Caprin-1 plays crucial roles not only in viral replication *in vitro* but also in pathogenesis in mice through the suppression of SG formation. (A) Huh7/Caprin-1-AcGFP cells were infected with JEV (WT or 9798A mutant) at an MOI of 1.0, and the cellular localizations of Caprin-1-AcGFP and JEV core protein were determined at 24 h postinfection by immunofluorescence analysis with rabbit anti-core PAb and AF594-conjugated anti-rabbit IgG. Cell nuclei were stained with DAPI (blue). (B) Focus formation of JEV (WT or 9798A mutant) in Vero cells incubated in methylcellulose overlay medium at 48 h postinfection. The infectious foci were immunostained as described previously (20). (C) Growth kinetics of JEV (WT or 9798A mutant) in C6/36 and Vero cells infected at an MOI of 0.1. Infectious titers in the culture supernatants harvested at the indicated times were determined by focus-forming assays in Vero cells. Means of three experiments are indicated. (D) Huh7/Caprin-1-AcGFP cells were infected with either WT or 9798A at an MOI of 0.5, and cellular localizations of Caprin-1-AcGFP, G3BP (blue), and JEV NS2B (red) were determined at 24 h postinfection by immunofluorescence analysis with mouse anti-G3BP MAb and rabbit anti-NS2B PAb, followed by AF633-conjugated anti-mouse IgG and AF594-conjugated anti-rabbit IgG, respectively. (E) Numbers >of G3BP-positive foci in 30 cells prepared as described in panel D were counted. Lines, boxes, and error bars indicate the means, 25th to 75th percentiles, and 95th percentiles, respectively. The significance of differences between the means was determined by Student's *t* test. *, $P < 0.01$. (F) Infectious titers in the cerebrums of mice at 7 days postintraperitoneal inoculation with 5×10^4 FFU/100 μl of either WT or 9798A virus were determined in Vero cells. The means of titers in the homogenates of the cerebrums from three mice are indicated. The detection limit is 10^2 FFU/g of cerebrum. (G) Percentages of surviving mice ($n = 10$) after intraperitoneal inoculation with 5×10^4 FFU of either WT or 9798A virus. Mock, inoculation with DMEM.

Caprin-1 exhibited reduced replication *in vitro* and attenuated pathogenicity in mice.

G3BP is one of the key molecules involved in the SG aggregation process and self-oligomerizes in a phosphorylation-dependent manner to sequester mRNA in SGs (4). Therefore, G3BP knocked down cells (6) and G3BP knockout mouse embryonic fibroblast cells are deficient in the SG formation. In addition, G3BP sequestration inhibits SG formation in response to arsenite treatment (32). Caprin-1, known as RNA granule protein 105 or p137 (33), also participates in SG formation through phosphorylation of eIF2α (28) and is ubiquitously expressed in the cytoplasm. Caprin-1 regulates the transport and translation of mRNAs

of proteins involved in the synaptic plasticity in neurons (34) and cellular proliferation and migration in multiple cell types (28) through an interaction with G3BP. USP10, another SG-associated molecule, also interacts with G3BP and forms the G3BP/USP10 complex (29), suggesting that several SG-associated RBPs participate in the formation of a protein-protein network. In this study, the JEV core protein was shown to directly interact with Caprin-1, to sequester several key molecule complexes involved in SG formation to the perinuclear region in cells infected with JEV, and to facilitate viral propagation through the suppression of SG formation.

Flaviviruses replicate at a relatively low rate in comparison with most of the other positive-stranded RNA viruses, and thus rapid shutdown of host cellular protein synthesis would be deleterious for the viral life cycle. In cells infected with JEV, several SG components were colocalized with the core protein in the perinuclear region, while in those infected with WNV or DENV, SG components were accumulated in a replication complex composed of viral RNA and nonstructural proteins. In addition, the phosphorylation of eIF2α induced by arsenite was completely canceled by the infection with WNV or DENV, whereas the suppression of the phosphorylation was limited in JEV infection (15). Incorporation of the nascent viral RNA into the membranous structure induced by viral nonstructural proteins prevents PKR activation and inhibits SG formation in cells infected with WNV (17). In cells infected with hepatitis C virus (HCV), which belongs to the genus *Hepacivirus* in the family *Flaviviridae*, induction of SG formation was observed in the early stage of infection, in contrast to the inhibition of the arsenite-induced SG formation in the late stage (35). Several SG components, such as G3BP1, PABP1, and ataxin-2, were colocalized with HCV core protein around lipid droplets (35), and G3BP1 was also associated with the NS5B protein and the 5′ terminus of the minus-strand viral RNA (36) to mediate efficient viral replication. Collectively, these data suggest that flaviviruses have evolved to regulate cellular processes involved in SG formation through various strategies.

PKR is one of the interferon-stimulated genes and plays a crucial role in antiviral defense through phosphorylation of eIF2α, which leads to host translational shutoff (37, 38). In the early stage of flavivirus infection, both positive- and negative-stranded RNAs transcribe at low levels, while genomic RNA predominantly synthesizes in the late stage of infection (39). It was shown that activation of PKR was suppressed (40) or only induced in the late stage of WNV infection (41) and impaired by the expression of HCV NS5A (42–44). Very recently, JEV NS2A was shown to suppress PKR activation through inhibition of dimerization of PKR in the early stage but not in the late stage of infection (45). In this study, we have shown that JEV core protein interacts with Caprin-1 and inhibits SG formation downstream of the phosphorylation of eIF2α in the late stage of infection, suggesting that JEV has evolved to escape from host antiviral responses in the multiple stages of viral replication by using structural and nonstructural proteins.

The flavivirus core protein is a multifunctional protein involved in many aspects of the viral life cycle. In addition to the formation of viral nucleocapsid through the interaction with viral RNA (as a structural protein) (46), flavivirus core proteins interact with various host factors, such as B23 (47), Jab1 (48), hnRNP K (49), and hnRNP A2 (23), and regulate viral replication and/or modify the host cell environment (as a nonstructural protein). Although further investigations are needed to clarify the precise mechanisms underlying the circumvention of SG formation through the interaction of JEV core protein with Caprin-1, leading to efficient propagation *in vitro* and pathogenicity in mice, these findings could help not only to provide new insight into strategies by which viruses escape host stress responses but also to develop novel antiviral agents for flavivirus infection.

ACKNOWLEDGMENTS

We thank M. Tomiyama for secretarial assistance. We also thank K. Saito and T. Wakita for technical advice and the infectious clone of JEV, respectively.

This work was supported in part by grants-in-aid from the Ministry of Health, Labor, and Welfare, the Ministry of Education, Culture, Sports, Science, and Technology, and the Osaka University Global Center of Excellence Program. H. Katoh is a research fellow of the Japanese Society for the Promotion of Science.

REFERENCES

1. **Nover L, Scharf KD, Neumann D.** 1989. Cytoplasmic heat shock granules are formed from precursor particles and are associated with a specific set of mRNAs. Mol. Cell. Biol. 9:1298–1308.
2. **Anderson P, Kedersha N.** 2002. Stressful initiations. J. Cell Sci. 115:3227–3234.
3. **Gilks N, Kedersha N, Ayodele M, Shen L, Stoecklin G, Dember LM, Anderson P.** 2004. Stress granule assembly is mediated by prion-like aggregation of TIA-1. Mol. Biol. Cell 15:5383–5398.
4. **Tourriere H, Chebli K, Zekri L, Courselaud B, Blanchard JM, Bertrand E, Tazi J.** 2003. The RasGAP-associated endoribonuclease G3BP assembles stress granules. J. Cell Biol. 160:823–831.
5. **Kedersha N, Cho MR, Li W, Yacono PW, Chen S, Gilks N, Golan DE, Anderson P.** 2000. Dynamic shuttling of TIA-1 accompanies the recruitment of mRNA to mammalian stress granules. J. Cell Biol. 151:1257–1268.
6. **White JP, Cardenas AM, Marissen WE, Lloyd RE.** 2007. Inhibition of cytoplasmic mRNA stress granule formation by a viral proteinase. Cell Host Microbe 2:295–305.
7. **Khaperskyy DA, Hatchette TF, McCormick C.** 2012. Influenza A virus inhibits cytoplasmic stress granule formation. FASEB J. 26:1629–1639.
8. **Abrahamyan LG, Chatel-Chaix L, Ajamian L, Milev MP, Monette A, Clement JF, Song R, Lehmann M, DesGroseillers L, Laughrea M, Boccaccio G, Mouland AJ.** 2010. Novel Staufen1 ribonucleoproteins prevent formation of stress granules but favour encapsidation of HIV-1 genomic RNA. J. Cell Sci. 123:369–383.
9. **McInerney GM, Kedersha NL, Kaufman RJ, Anderson P, Liljestrom P.** 2005. Importance of eIF2α phosphorylation and stress granule assembly in alphavirus translation regulation. Mol. Biol. Cell 16:3753–3763.
10. **Smith JA, Schmechel SC, Raghavan A, Abelson M, Reilly C, Katze MG, Kaufman RJ, Bohjanen PR, Schiff LA.** 2006. Reovirus induces and benefits from an integrated cellular stress response. J. Virol. 80:2019–2033.
11. **Katsafanas GC, Moss B.** 2007. Colocalization of transcription and translation within cytoplasmic poxvirus factories coordinates viral expression and subjugates host functions. Cell Host Microbe 2:221–228.
12. **Misra UK, Kalita J.** 2010. Overview: Japanese encephalitis. Prog. Neurobiol. 91:108–120.
13. **Sumiyoshi H, Mori C, Fuke I, Morita K, Kuhara S, Kondou J, Kikuchi Y, Nagamatu H, Igarashi A.** 1987. Complete nucleotide sequence of the Japanese encephalitis virus genome RNA. Virology 161:497–510.
14. **Murray CL, Jones CT, Rice CM.** 2008. Architects of assembly: roles of *Flaviviridae* non-structural proteins in virion morphogenesis. Nat. Rev. Microbiol. 6:699–708.
15. **Emara MM, Brinton MA.** 2007. Interaction of TIA-1/TIAR with West Nile and dengue virus products in infected cells interferes with stress granule formation and processing body assembly. Proc. Natl. Acad. Sci. U. S. A. 104:9041–9046.
16. **Li W, Li Y, Kedersha N, Anderson P, Emara M, Swiderek KM, Moreno GT, Brinton MA.** 2002. Cell proteins TIA-1 and TIAR interact with the 3′ stem-loop of the West Nile virus complementary minus-strand RNA and facilitate virus replication. J. Virol. 76:11989–12000.
17. **Courtney SC, Scherbik SV, Stockman BM, Brinton MA.** 2012. West Nile

virus infections suppress early viral RNA synthesis and avoid inducing the cell stress granule response. J. Virol. 86:3647–3657.
18. Kambara H, Tani H, Mori Y, Abe T, Katoh H, Fukuhara T, Taguwa S, Moriishi K, Matsuura Y. 2011. Involvement of cyclophilin B in the replication of Japanese encephalitis virus. Virology 412:211–219.
19. Mori Y, Yamashita T, Tanaka Y, Tsuda Y, Abe T, Moriishi K, Matsuura Y. 2007. Processing of capsid protein by cathepsin L plays a crucial role in replication of Japanese encephalitis virus in neural and macrophage cells. J. Virol. 81:8477–8487.
20. Mori Y, Okabayashi T, Yamashita T, Zhao Z, Wakita T, Yasui K, Hasebe F, Tadano M, Konishi E, Moriishi K, Matsuura Y. 2005. Nuclear localization of Japanese encephalitis virus core protein enhances viral replication. J. Virol. 79:3448–3458.
21. Kambara H, Fukuhara T, Shiokawa M, Ono C, Ohara Y, Kamitani W, Matsuura Y. 2012. Establishment of a novel permissive cell line for the propagation of hepatitis C virus by expression of microRNA miR122. J. Virol. 86:1382–1393.
22. Zhao Z, Date T, Li Y, Kato T, Miyamoto M, Yasui K, Wakita T. 2005. Characterization of the E-138 (Glu/Lys) mutation in Japanese encephalitis virus by using a stable, full-length, infectious cDNA clone. J. Gen. Virol. 86:2209–2220.
23. Katoh H, Mori Y, Kambara H, Abe T, Fukuhara T, Morita E, Moriishi K, Kamitani W, Matsuura Y. 2011. Heterogeneous nuclear ribonucleoprotein A2 participates in the replication of Japanese encephalitis virus through an interaction with viral proteins and RNA. J. Virol. 85:10976–10988.
24. Hamamoto I, Nishimura Y, Okamoto T, Aizaki H, Liu M, Mori Y, Abe T, Suzuki T, Lai MM, Miyamura T, Moriishi K, Matsuura Y. 2005. Human VAP-B is involved in hepatitis C virus replication through interaction with NS5A and NS5B. J. Virol. 79:13473–13482.
25. Jones CT, Ma L, Burgner JW, Groesch TD, Post CB, Kuhn RJ. 2003. Flavivirus capsid is a dimeric alpha-helical protein. J. Virol. 77:7143–7149.
26. Ward AM, Bidet K, Yinglin A, Ler SG, Hogue K, Blackstock W, Gunaratne J, Garcia-Blanco MA. 2011. Quantitative mass spectrometry of DENV-2 RNA-interacting proteins reveals that the DEAD-box RNA helicase DDX6 binds the DB1 and DB2 3′ UTR structures. RNA Biol. 8:1173–1186.
27. Ma L, Jones CT, Groesch TD, Kuhn RJ, Post CB. 2004. Solution structure of dengue virus capsid protein reveals another fold. Proc. Natl. Acad. Sci. U. S. A. 101:3414–3419.
28. Solomon S, Xu Y, Wang B, David MD, Schubert P, Kennedy D, Schrader JW. 2007. Distinct structural features of Caprin-1 mediate its interaction with G3BP-1 and its induction of phosphorylation of eukaryotic translation initiation factor 2α, entry to cytoplasmic stress granules, and selective interaction with a subset of mRNAs. Mol. Cell. Biol. 27:2324–2342.
29. Soncini C, Berdo I, Draetta G. 2001. Ras-GAP SH3 domain binding protein (G3BP) is a modulator of USP10, a novel human ubiquitin specific protease. Oncogene 20:3869–3879.
30. Montero H, Rojas M, Arias CF, Lopez S. 2008. Rotavirus infection induces the phosphorylation of eIF2α but prevents the formation of stress granules. J. Virol. 82:1496–1504.
31. Sola I, Galan C, Mateos-Gomez PA, Palacio L, Zuniga S, Cruz JL, Almazan F, Enjuanes L. 2011. The polypyrimidine tract-binding protein affects coronavirus RNA accumulation levels and relocalizes viral RNAs to novel cytoplasmic domains different from replication-transcription sites. J. Virol. 85:5136–5149.
32. Hinton SD, Myers MP, Roggero VR, Allison LA, Tonks NK. 2010. The pseudophosphatase MK-STYX interacts with G3BP and decreases stress granule formation. Biochem. J. 427:349–357.
33. Grill B, Wilson GM, Zhang KX, Wang B, Doyonnas R, Quadroni M, Schrader JW. 2004. Activation/division of lymphocytes results in increased levels of cytoplasmic activation/proliferation-associated protein-1: prototype of a new family of proteins. J. Immunol. 172:2389–2400.
34. Shiina N, Shinkura K, Tokunaga M. 2005. A novel RNA-binding protein in neuronal RNA granules: regulatory machinery for local translation. J. Neurosci. 25:4420–4434.
35. Ariumi Y, Kuroki M, Kushima Y, Osugi K, Hijikata M, Maki M, Ikeda M, Kato N. 2011. Hepatitis C virus hijacks P-body and stress granule components around lipid droplets. J. Virol. 85:6882–6892.
36. Yi Z, Pan T, Wu X, Song W, Wang S, Xu Y, Rice CM, Macdonald MR, Yuan Z. 2011. Hepatitis C virus co-opts Ras-GTPase-activating protein-binding protein 1 for its genome replication. J. Virol. 85:6996–7004.
37. Gale M, Jr, Katze MG. 1998. Molecular mechanisms of interferon resistance mediated by viral-directed inhibition of PKR, the interferon-induced protein kinase. Pharmacol. Ther. 78:29–46.
38. Pindel A, Sadler A. 2011. The role of protein kinase R in the interferon response. J. Interferon Cytokine Res. 31:59–70.
39. Chu PW, Westaway EG. 1985. Replication strategy of Kunjin virus: evidence for recycling role of replicative form RNA as template in semiconservative and asymmetric replication. Virology 140:68–79.
40. Elbahesh H, Scherbik SV, Brinton MA. 2011. West Nile virus infection does not induce PKR activation in rodent cells. Virology 421:51–60.
41. Samuel MA, Whitby K, Keller BC, Marri A, Barchet W, Williams BR, Silverman RH, Gale M, Jr, Diamond MS. 2006. PKR and RNase L contribute to protection against lethal West Nile Virus infection by controlling early viral spread in the periphery and replication in neurons. J. Virol. 80:7009–7019.
42. Gale M, Jr, Blakely CM, Kwieciszewski B, Tan SL, Dossett M, Tang NM, Korth MJ, Polyak SJ, Gretch DR, Katze MG. 1998. Control of PKR protein kinase by hepatitis C virus nonstructural 5A protein: molecular mechanisms of kinase regulation. Mol. Cell. Biol. 18:5208–5218.
43. Gale MJ, Jr, Korth MJ, Tang NM, Tan SL, Hopkins DA, Dever TE, Polyak SJ, Gretch DR, Katze MG. 1997. Evidence that hepatitis C virus resistance to interferon is mediated through repression of the PKR protein kinase by the nonstructural 5A protein. Virology 230:217–227.
44. He Y, Tan SL, Tareen SU, Vijaysri S, Langland JO, Jacobs BL, Katze MG. 2001. Regulation of mRNA translation and cellular signaling by hepatitis C virus nonstructural protein NS5A. J. Virol. 75:5090–5098.
45. Tu YC, Yu CY, Liang JJ, Lin E, Liao CL, Lin YL. 2012. Blocking dsRNA-activated protein kinase PKR by Japanese encephalitis virus nonstructural protein 2A. J. Virol. 86:10347–10358.
46. Khromykh AA, Westaway EG. 1996. RNA binding properties of core protein of the flavivirus Kunjin. Arch. Virol. 141:685–699.
47. Tsuda Y, Mori Y, Abe T, Yamashita T, Okamoto T, Ichimura T, Moriishi K, Matsuura Y. 2006. Nucleolar protein B23 interacts with Japanese encephalitis virus core protein and participates in viral replication. Microbiol. Immunol. 50:225–234.
48. Oh W, Yang MR, Lee EW, Park KM, Pyo S, Yang JS, Lee HW, Song J. 2006. Jab1 mediates cytoplasmic localization and degradation of West Nile virus capsid protein. J. Biol. Chem. 281:30166–30174.
49. Chang CJ, Luh HW, Wang SH, Lin HJ, Lee SC, Hu ST. 2001. The heterogeneous nuclear ribonucleoprotein K (hnRNP K) interacts with dengue virus core protein. DNA Cell Biol. 20:569–577.

Zinc-finger antiviral protein mediates retinoic acid inducible gene I–like receptor-independent antiviral response to murine leukemia virus

Hanna Lee[a,b], Jun Komano[c], Yasunori Saitoh[d], Shoji Yamaoka[d], Tatsuya Kozaki[a,b], Takuma Misawa[a,b], Michihiro Takahama[a,b], Takashi Satoh[a,b], Osamu Takeuchi[e], Naoki Yamamoto[f], Yoshiharu Matsuura[g], Tatsuya Saitoh[a,b,1], and Shizuo Akira[a,b,1]

[a]Laboratory of Host Defense, World Premier International Immunology Frontier Research Center, Osaka University, Osaka 565-0871, Japan; Departments of [b]Host Defense and [g]Molecular Virology, Research Institute for Microbial Diseases, Osaka University, Osaka 565-0871, Japan; [c]Department of Infectious Diseases, Osaka Prefectural Institute of Public Health, Osaka 537-0025, Japan; [d]Department of Molecular Virology, Graduate School of Medical and Dental Sciences, Tokyo Medical and Dental University, Tokyo 113-8519, Japan; [e]Laboratory of Infection and Prevention, Institute for Virus Research, Kyoto University, Kyoto 606-8507, Japan; and [f]Department of Microbiology, Yong Loo Lin School of Medicine, National University of Singapore, Singapore 117599

Contributed by Shizuo Akira, June 5, 2013 (sent for review May 14, 2013)

When host cells are infected by an RNA virus, pattern-recognition receptors (PRRs) recognize the viral RNA and induce the antiviral innate immunity. Toll-like receptor 7 (TLR7) detects the genomic RNA of incoming murine leukemia virus (MLV) in endosomes and mediates the antiviral response. However, the RNA-sensing PRR that recognizes the MLV in the cytosol is not fully understood. Here, we definitively demonstrate that zinc-finger antiviral protein (ZAP) acts as a cytosolic RNA sensor, inducing the degradation of the MLV transcripts by the exosome, an RNA degradation system, on RNA granules. Although the retinoic acid inducible gene I (RIG-I)–like receptors (RLRs) RIG-I and melanoma differentiation-associated protein 5 detect various RNA viruses in the cytosol and induce the type I IFN-dependent antiviral response, RLR loss does not alter the replication efficiency of MLV. In sharp contrast, the loss of ZAP greatly enhances the replication efficiency of MLV. ZAP localizes to RNA granules, where the processing-body and stress-granule proteins assemble. ZAP induces the recruitment of the MLV transcripts and exosome components to the RNA granules. The CCCH-type zinc-finger domains of ZAP, which are RNA-binding motifs, mediate its localization to RNA granules and MLV transcripts degradation by the exosome. Although ZAP was known as a regulator of RIG-I signaling in a human cell line, ZAP deficiency does not affect the RIG-I–dependent production of type I IFN in mouse cells. Thus, ZAP is a unique member of the cytosolic RNA-sensing PRR family that targets and eliminates intracellular RNA viruses independently of TLR and RLR family members.

host defense | retrovirus | ZC3HAV1

Innate immunity is induced after the recognition of viral RNAs by pattern-recognition receptors (PRRs) and is the first line of the host defenses against a variety of RNA viruses (1, 2). Among the PRRs, the Toll-like receptor (TLR) and retinoic acid-inducible gene I (RIG-I)-like receptor (RLR) families play major roles in the recognition of viral RNAs. The RLR's RIG-I [also called DEAD (Asp-Glu-Ala-Asp) box polypeptide 58 (DDX58)] and melanoma differentiation-associated protein 5 [MDA5, also called interferon induced with helicase C domain 1 (IFIH1)] are RNA helicases that sense the ds form of viral RNAs in the cytosol (3, 4). After sensing dsRNA, the RLRs trigger a signaling pathway that activates interferon (IFN) regulatory factor 3 (IRF3) and IRF7, transcription factors that induce IFN stimulation-responsive, element-dependent transcription (5, 6). This results in the production of type I IFN and the expression of IFN-inducible antiviral proteins. The sensing of viral RNAs by TLR family members also induces the IRF3- and IRF7-dependent type I IFN response (1, 2). In epithelial cells, TLR3, a sensor of dsRNA, detects the incoming RNA virus genomes in endosomes and induces the activation of IRF3, leading to the production of type I IFN (7, 8). In plasmacytoid dendritic cells, TLR7, a sensor of single-stranded (ss) RNA, detects incoming RNA virus genomes in endo-lysosomes and triggers the activation of IRF7, leading to the robust production of type I IFN (9–13). Thus, TLRs and RLRs play major roles in the establishment of an antiviral state by mediating the production of type I IFN.

Murine leukemia virus (MLV), a retrovirus belonging to the gammaretroviral genus of the family *Retroviridae*, is a causative agent of cancer in murine hosts (14, 15). Although type I IFN is essential for the protection of hosts from lethal infection with a variety of RNA viruses, such as influenza A virus (IAV) and vesicular stomatitis virus (VSV), type I IFN is not essential for induction of the antiviral state against MLV (16–18). Therefore, a different type of innate immune system has been proposed to protect hosts from MLV infection. Although TLR7 has been shown to induce virus-neutralizing immunity after MLV genomic RNA is detected in endosomes (16), the RNA sensor responsible for the elimination of MLV in the cytosol has not been fully understood. RLRs are candidate RNA sensors of intracellular MLV. RLRs might mediate the antiviral response to MLV after the viral RNA is detected, independently of type I IFN because RLRs stimulate not only IRF3/IRF7, but also other transcription factors, such as NF-κB and activator protein 1, which are responsible for the production of inflammatory cytokines and chemokines (19). Another candidate sensor is zinc-finger antiviral protein [ZAP, also called zinc finger CCCH-type, antiviral 1 (ZC3HAV1)]. ZAP was originally identified with an expression cloning method as one of the antiviral proteins directed against MLV (20). ZAP reduces the level of MLV transcripts in the cytosol to suppress MLV infection at the posttranscriptional stage, whereas ZAP does not inhibit the early stage of the MLV infection. ZAP recognizes the MLV transcripts via its CCCH-type zinc-finger domains and binds with RNA helicases and the components of the exosome (an RNA degradation system) to induce the degradation of the MLV transcripts (21–25). However, it is unclear whether endogenous ZAP is involved in the antiviral response to replication-competent MLV in primary cells. In the present study, we examined the roles of these two types of cytosolic RNA sensors and demonstrated the spatial regulation of the innate immune response directed against intracellular MLV.

Author contributions: T. Saitoh and S.A. designed research; H.L., J.K., Y.S., S.Y., T.K., T.M., M.T., T. Satoh, O.T., N.Y., and Y.M. performed research; and T. Saitoh wrote the paper.

The authors declare no conflict of interest.

[1]To whom correspondence may be addressed. E-mail: sakira@biken.osaka-u.ac.jp or tatsuya@biken.osaka-u.ac.jp.

This article contains supporting information online at www.pnas.org/lookup/suppl/doi:10.1073/pnas.1310604110/-/DCSupplemental.

Results

RLRs Do Not Regulate the Antiviral Response to MLV in Primary Mouse Embryonic Fibroblasts. We first examined the involvement of RLRs in the antiviral response to MLV in mouse embryonic fibroblasts (MEFs). The replication efficiency of MLV in *Ddx58*$^{-/-}$/*Ifih1*$^{-/-}$ MEFs was similar to that in *Ddx58*$^{+/+}$/*Ifih1*$^{+/+}$ MEFs (Fig. 1*A*). Furthermore, the replication efficiency of MLV in *Irf3*$^{-/-}$/*Irf7*$^{-/-}$ MEFs was similar to that in *Irf3*$^{+/-}$/*Irf7*$^{+/-}$ MEFs (Fig. 1*B*). Consistent with this, the levels of *Ifnb1* and *chemokine (C-X-C motif) ligand 10* (*Cxcl10*) mRNAs did not change during MLV infection (Fig. 1 *C–F*). The RLR–IRF3/7 signaling axis is essential for the up-regulation of *Ifnb1* and *Cxcl10* mRNAs during VSV infection. R848, a ligand of TLR7, failed to stimulate MEFs isolated from C57BL/6 mice (Fig. S1), indicating that no RNA-sensing TLR family member recognizes MLV in the extracellular space of MEFs. Therefore, MLV evades the RLR and TLR systems and does not induce the type I IFN response in MEFs.

Endogenous ZAP Limits the Replication of MLV in Primary MEFs. We next investigated the role of ZAP, another cytosolic sensor of viral RNA, in the antiviral response to MLV. Previous studies have demonstrated that the ectopic expression of ZAP potently inhibits replication-incompetent MLV in the cytoplasm of various types of cell lines (20). Therefore, we generated *Zc3hav1*$^{-/-}$ mice to examine whether endogenous ZAP controls the replication of MLV in primary cells (Fig. S2). Detectable levels of ZAP protein were expressed in *Zc3hav1*$^{+/+}$ MEFs before and after MLV infection (Fig. S2*D*). Whereas ZAP deficiency did not alter the replication efficiency of VSV in MEFs (Fig. S3), ZAP deficiency greatly enhanced the replication efficiency of MLV (Fig. 2 *A* and *B*). These findings indicate that endogenous ZAP is responsible for the antiviral response to replication-competent MLV in primary mouse cells.

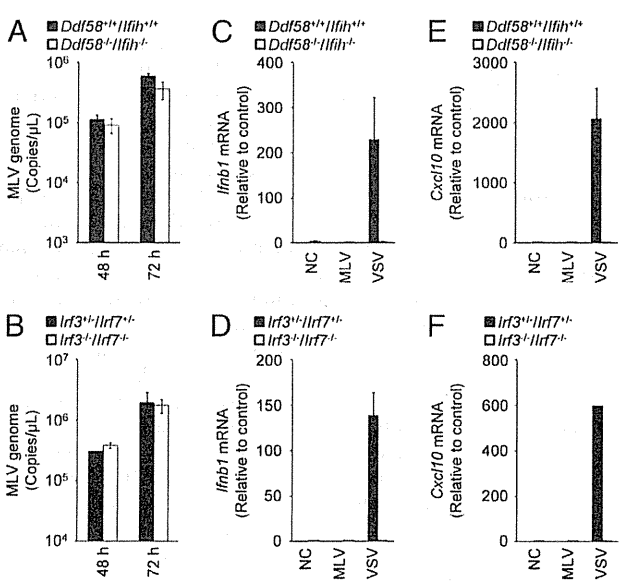

Fig. 1. RIG-I–like receptors are not essential for the antiviral response to MLV in primary MEFs. (*A* and *B*) *Ddx58*$^{+/+}$/*Ifih1*$^{+/+}$ and *Ddx5*$^{-/-}$/*Ifih1*$^{-/-}$ MEFs (*A*) or *Irf3*$^{+/-}$/*Irf7*$^{+/-}$ and *Irf*$^{-/-}$/*Irf7*$^{-/-}$ MEFs (*B*) were infected with MLV (2×10^{10} copies per μL) for 48 or 72 h. The copy numbers of the MLV genome in the culture supernatants were measured by quantitative RT-PCR. (*C–F*) *Ddx58*$^{+/+}$/*Ifih1*$^{+/+}$ and *Ddx58*$^{-/-}$/*Ifih1*$^{-/-}$ MEFs (*C* and *E*) or *Irf3*$^{+/-}$/*Irf7*$^{+/-}$ and *Irf3*$^{-/-}$/*Irf7*$^{-/-}$ MEFs (*D* and *F*) were infected with MLV (2×10^{10} copies per μL) or VSV [multiplicity of infection (MOI) = 1] for 12 h. The levels of *Ifnb1* (*C* and *D*) and *Cxcl10* (*E* and *F*) mRNAs were measured by quantitative RT-PCR. The results shown are means ± SD ($n = 3$).

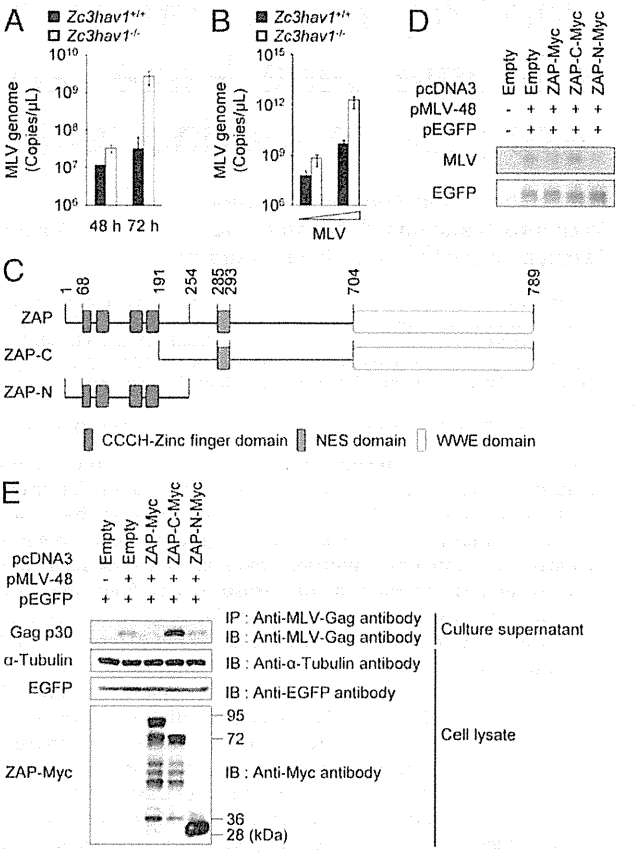

Fig. 2. ZAP inhibits MLV replication in primary MEFs. (*A*) *Zc3hav1*$^{+/+}$ and *Zc3hav1*$^{-/-}$ MEFs were infected with MLV (2×10^{10} copies per μL). Viral RNA was isolated at the indicated time points. The copy numbers of the MLV genome in the culture supernatants were measured by quantitative RT-PCR. (*B*) *Zc3hav1*$^{+/+}$ and *Zc3hav1*$^{-/-}$ MEFs were infected with increasing doses of MLV (2×10^{8} and 2×10^{9} copies per μL) for 96 h. The copy numbers of the MLV genome in the culture supernatants were measured by quantitative RT-PCR. (*C*) Domain architecture of ZAP. (*D* and *E*) 293T cells were transfected with pMLV-48 and pEGFP-N1 together with the indicated ZAP expression plasmids for 48 h. Cytoplasmic RNA was subjected to Northern blotting analysis of the indicated RNAs (*D*). The culture supernatants were subjected to immunoprecipitation coupled to immunoblotting to detect the indicated proteins (*E*). The results shown are means ± SD ($n = 3$). NES, nuclear export signal.

The CCCH-type zinc-finger domains of ZAP are known to recognize the MLV transcripts and to induce its degradation (21, 25). Consistent with this, the ectopic expression of the N-terminal portion of ZAP, which contains the CCCH-type zinc-finger domains, but not the ectopic expression of the C-terminal portion of ZAP, which lacks CCCH-type zinc-finger domains, reduced the level of MLV transcripts in the cytosol (Fig. 2 *C* and *D*). The ectopic expression of the CCCH-type zinc-finger domains of ZAP also suppressed the expression of the Gag protein of MLV (Fig. 2*E*). Therefore, the CCCH-type zinc-finger domains of ZAP are essential for its antiviral action against MLV.

CCCH-Type Zinc-Finger Domains of ZAP Mediate Its Localization to the RNA Granules. The involvement of ZAP in the antiviral response to MLV prompted us to determine the mechanism underlying the ZAP-dependent degradation of the MLV transcripts. Although a previous study showed that ZAP acts in the cytosol (20), it was still unclear where in the cytosol ZAP eliminates the MLV transcripts. Therefore, we examined whether ZAP localizes to a cytosolic compartment, such as in the processing bodies

(P-bodies) (26). When it was ectopically expressed, ZAP localized to cytoplasmic dot-like structures in a manner that was dependent on its CCCH-type zinc-finger domains (Fig. 3*A*). The ZAP-positive dot-like structures colocalized with marker proteins for P-bodies, such as DCP1 decapping enzyme homolog A (*Saccharomyces cerevisiae*; DCP1A) and DDX6 (Fig. 3*B*). ZAP induced the enlargement of the DCP1A- and DDX6-positive dot-like structures, suggesting that the ZAP-positive dot-like structures are not conventional P-bodies. ZAP also colocalized with marker proteins for stress granules, such as GTPase-activating protein (SH3 domain) binding protein 1 (G3BP1) and cytotoxic granule-associated RNA binding protein (TIA-1) (Fig. S4). Furthermore, the RNA helicase DEAH (Asp-Glu-Ala-His) box polypeptide 30 (DHX30), which binds to ZAP to facilitate its antiviral action against MLV (24), colocalized with ZAP to the DCP1A-positive dot-like structures (Fig. S5). By contrast, ZAP did not colocalize with mitochondrial preprotein translocases of the outer membrane 20 (TOM20), 70-kDa peroxisomal membrane protein (PMP70), early endosome antigen 1 (EEA1), or lysosomal-associated membrane protein 1 (LAMP1), marker proteins for the mitochondria, peroxisomes, endosomes, and lysosomes, respectively (Fig. 3*C*). These findings indicate that ZAP localizes to the RNA granules, where the marker proteins for P-bodies and stress granules assemble.

ZAP Recruits the MLV Transcripts and Exosome Components to RNA Granules. The localization of the MLV transcripts has been poorly understood. We used an improved RNA FISH method to visualize the subcellular localization of viral RNA and identified the cytosolic compartments in which ZAP acts on the MLV transcripts. The MLV transcripts mainly localize in the cytosol and colocalize with DCP1A-positive RNA granules at low frequency (Fig. 4). However, the ectopic expression of ZAP reduced the level of MLV transcripts in the cytosol and dramatically altered its localization from the cytosol to ZAP- and DCP1A-positive RNA granules (Fig. 4 and Fig. S6). Therefore, ZAP tethers the MLV transcripts and transfers it to the RNA granules.

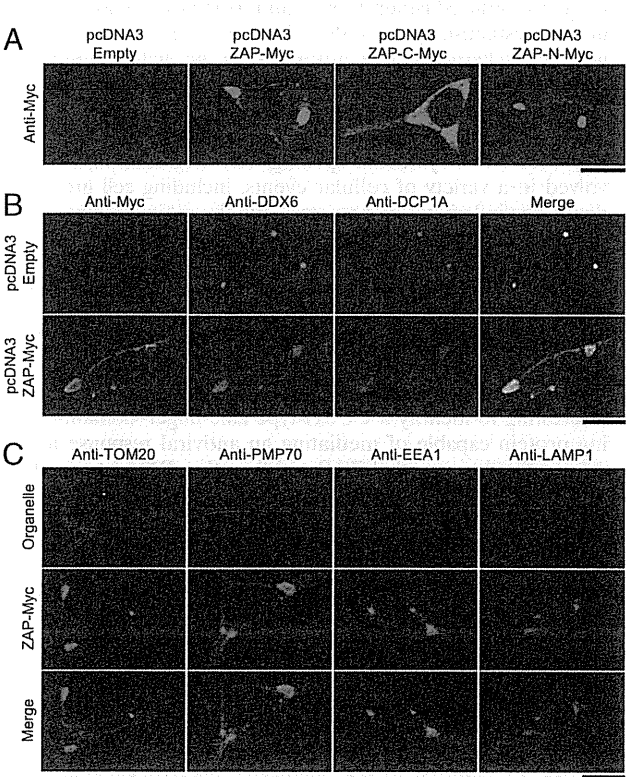

Fig. 3. ZAP localizes to DCP1A- and DDX6-positive RNA granules. (*A–C*) 293T cells were transfected with the indicated vectors for 48 h and then fixed. The samples were immunostained with the indicated antibodies and then observed by confocal laser scanning microscopy. The data are representative of three independent experiments. (Scale bars, 10 μm.)

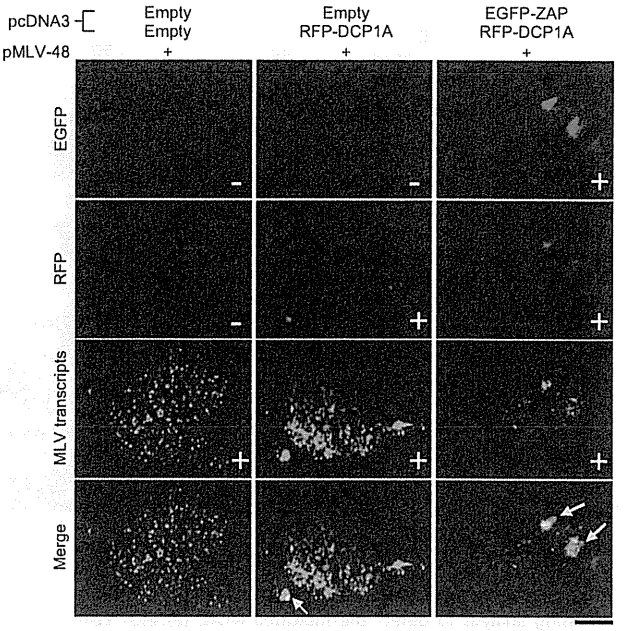

Fig. 4. ZAP recruits the MLV transcripts to RNA granules. 293T cells were transfected with the indicated plasmids for 48 h and then fixed. The samples were subjected to in situ hybridization analysis with a fluorescent probe for MLV transcripts and then observed by confocal laser scanning microscopy. (Scale bar, 10 μm.)

Because ZAP is not a ribonuclease, it requires the support of an RNA degradation system to destabilize the MLV transcripts. Consistent with this, previous studies have shown that exosome components and RNA helicases interact with ZAP to mediate the antiviral response to MLV (22–24). Therefore, we focused on the localization of exosome component 5 (EXOSC5, also known as RRP46) (27). The ectopic expression of EXOSC5 reduced the level of MLV transcripts in the cytosol (Fig. 5*A*). Under normal conditions, EXOSC5 localized in the cytosol and nuclei, and colocalized with the DCP1A-positive RNA granules at low frequency (Fig. 5*B*). However, when ZAP was ectopically expressed, EXOSC5 moved from the cytosol to the ZAP- and DCP1A-positive RNA granules (Fig. 5*B*). These findings indicate that ZAP recruits the exosome component to the RNA granules to induce the degradation of MLV transcripts.

ZAP Does Not Regulate the RIG-I–Dependent Type I IFN Response in Primary Mouse Cells. A recent study showed that ZAP positively regulated RIG-I signaling during RNA virus infection in a human cell line (28). Therefore, we examined the involvement of ZAP in the RIG-I–dependent type I IFN response in primary mouse cells. In *Zc3hav1*$^{-/-}$ primary MEFs, the IFN-β and Cxcl10 proteins were produced normally in response to VSV, an RNA virus recognized by RIG-I (Fig. 6 *A* and *B*). Although ZAP deficiency greatly enhanced the replication of MLV (Fig. 2 *A* and *B*), no IFN-β or Cxcl10 protein was produced in *Zc3hav1*$^{-/-}$ MEFs infected with MLV. In *Zc3hav1*$^{-/-}$ mouse primary dendritic cells, IFN-β and Cxcl10 were also normally produced in response to

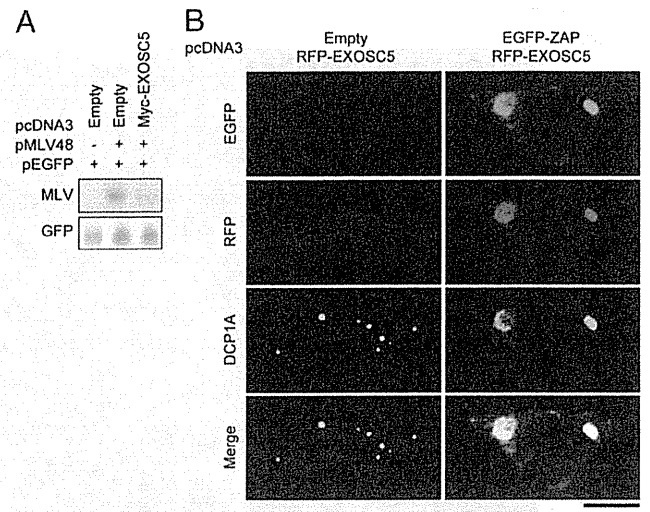

Fig. 5. EXOSC5 colocalizes with ZAP on RNA granules. (*A*) 293T cells were transfected with pMLV-48 and pEGFP-N1 together with the indicated ZAP expression plasmids for 48 h. Cytoplasmic RNA was subjected to Northern blotting analysis to detect the indicated RNAs. (*B*) 293T cells were transfected with the indicated plasmids and then fixed. The samples were immunostained with anti-DCP1A antibody and then observed by confocal laser scanning microscopy. The data are representative of three independent experiments. (Scale bar, 10 μm.)

Newcastle disease virus (NDV) and IAV, RNA viruses recognized by RIG-I (Fig. 6 *C* and *D*). Furthermore, ZAP deficiency did not affect the production of IFN-β in MEFs stimulated with the RIG-I ligand, 5′ triphosphate dsRNA (3pRNA) (Fig. S7 *A* and *B*), the MDA5 ligand poly(rI–rC), and a synthetic dsDNA poly(dA–dT) (Fig. S7*C*). These findings indicate that ZAP is not a regulator of the RIG-I–dependent type I IFN response in primary mouse cells and strengthen our conclusion that ZAP eliminates MLV independently of the RLR–IRF3/7 signaling axis.

Discussion

In this study, we showed that endogenous ZAP suppresses the replication of MLV in MEFs. This raises the issue of whether endogenous ZAP suppresses the replication of other types of RNA viruses, including human retroviruses. The RNAi-mediated knockdown of *ZC3HAV1* mRNA enhanced the replication of xenotropic MLV-related virus, an artificial retrovirus belonging to the gammaretroviral genus of the family *Retroviridae* (29), in 293T cells (Fig. S8 *A* and *B*), whereas the knockdown of *ZC3HAV1* mRNA did not enhance the replication of human T-cell leukemia virus type I, a retrovirus belonging to the deltaretroviral genus of the family *Retroviridae* (30), in MT-2 cells (Fig. S8 *C* and *D*). In a previous study, the knockdown of *ZC3HAV1* mRNA enhanced the replication of HIV-1, a retrovirus belonging to the lentiviral genus of the family *Retroviridae* (31), in HOS-CD4 cells expressing chemokine (C-C motif) receptor 5 (32). Therefore, ZAP functions in human cells to target not all but certain types of retroviruses. ZAP is also known to suppress the replication of RNA viruses belonging to the families *Filoviridae* and *Togaviridae* (33, 34). Although ZAP has been shown to recognize the viral RNA of RNA viruses belonging to the families *Filoviridae*, *Togaviridae*, and *Retroviridae via*, its CCCH-type zinc-finger domains, the common features that are recognized by these domains, such as specific sequences or structural characteristics, have not been determined. Further studies are required to identify the RNA ligand of ZAP that induces the destabilization of the viral RNA by the RNA degradation machinery.

Although accumulating evidence indicates that ZAP counters a variety of RNA viruses under in vitro experimental conditions (20, 33, 34), it is still unclear whether ZAP protects hosts from RNA viral infections in vivo. RNA-sensing TLRs and the ssDNA cytosine deaminase apolipoprotein B mRNA-editing, enzyme-catalytic, polypeptide-like 3 are other antiviral systems that affect mouse retroviruses, and also control the replication of endogenous retroviruses (ERVs) (16, 35–37). Therefore, ZAP might also contribute to the antiviral response to ERVs and prevent the ERV-induced generation of tumors in vivo. To assess this, we are now establishing a colony of *Zc3hav1*$^{-/-}$ mice in the C57BL/6 genetic background. In a future study, we will attempt to determine the in vivo role of ZAP in the host defense responses to endogenous and exogenous microbes.

The CCCH-type zinc-finger–domain-containing protein family regulates RNA synthesis, splicing, and degradation, and is involved in a variety of cellular events, including cell growth, cell death, the inflammatory response, and the antimicrobial response (38, 39). To date, more than 50 CCCH-type zinc-finger-domain–containing proteins have been identified (40). Although various CCCH-type zinc-finger-domain-containing proteins, including tristetraprolin, roquin, and regnase-1, have been shown to be regulators of cytokine mRNA stability, ZAP is the only CCCH-type zinc-finger–domain-containing protein known to promote the destabilization of viral RNA (20, 41–43). Therefore, it will be interesting to identify a CCCH-type zinc-finger–domain-containing protein capable of mediating an antiviral response to RNA viruses that have evaded ZAP and the other RNA-sensing PRRs.

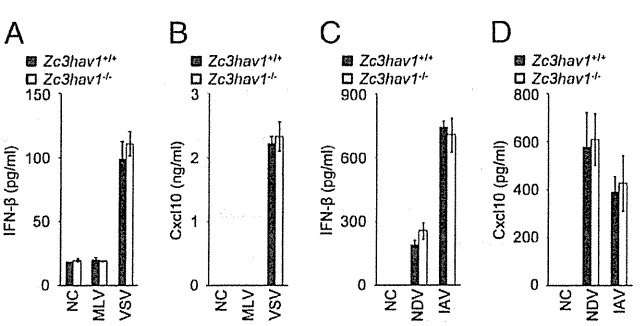

Fig. 6. ZAP is not essential for the RIG-I–mediated type I IFN response. (*A* and *B*) *Zc3hav1*$^{+/+}$ and *Zc3hav1*$^{-/-}$ MEFs were infected with MLV (2×10^{10} copies per μL) or VSV (MOI = 1) for 12 h. The levels of IFN-β (*A*) and Cxcl10 (*B*) proteins in the culture supernatants were measured with ELISAs. (*C* and *D*) *Zc3hav1*$^{+/+}$ and *Zc3hav1*$^{-/-}$ bone marrow-derived dendritic cells were infected with NDV (2.5×10^5 pfu/mL) or IAV (PR8, 100 Hematoglutinin) for 24 h. The levels of IFN-β (*C*) and Cxcl10 (*D*) proteins in the culture supernatants were measured with ELISAs. The results shown are means ± SD ($n = 3$).

Materials and Methods

Reagents. Anti-MLV-Gag antibody (ABIN457547) was purchased from Antibodies-online. Anti–α-tubulin antibody (T6199) was purchased from Sigma. Anti-GFP antibody (598) was purchased from MBL. Chicken anti–avian myelocytomatosis viral oncogene homolog (Myc) antibody (A190-103A) for the immunostaining assay was purchased from Bethyl Laboratories. Mouse anti–Myc-tag antibody (22765) for immunoblotting was purchased from Cell Signaling. Anti-DDX6 (ab40684), anti-PMP70 (ab3421), and anti-LAMP1 (ab24170) antibodies were purchased from Abcam. Anti-DCP1A antibody (H00055802-M06) was purchased from Abnova. Anti-TOM20 antibody (SC-11415) was purchased from Santa Cruz Biotechnology. Anti-EEA1 antibody (610456) was purchased from BD Biosciences. The ELISA kit for mouse IFN-β was purchased from Pestka Biomedical Laboratories Interferon Source. The ELISA kit for mouse Cxcl10 was purchased from R&D Systems.

Plasmids. pMLV-48 (GenBank accession no. J02255.1) was previously described (44) and kindly donated by H. Fan (University of California, Irvine, CA). pcDNA3.1(+) was purchased from Invitrogen. To generate the ZAP

expression constructs, NheI/NotI cDNA fragments encoding full-length mouse ZAP (GenBank accession no. NM_028864.2) and the C-terminal portion of ZAP and a BamHI/NotI cDNA fragment encoding the N-terminal portion of ZAP were amplified from pCMV-SPORT6-Zc3hav1 (MMM1013-7511214, Open Biosystems) by PCR and cloned into the corresponding restriction sites of pcDNA3 to produce pcDNA3-ZAP, pcDNA3-ZAP-C, and pcDNA3-ZAP-N, respectively. To generate the expression construct for the EGFP-ZAP fusion protein, an NheI/SpeI cDNA fragment encoding EGFP was amplified from pEGFP-N1 (Clontech) by PCR and cloned into the NheI site of pcDNA3-ZAP to produce pcDNA3-EGFP-ZAP. To generate the red fluorescent protein (RFP) expression construct, a BamHI/EcoRI cDNA fragment of RFP was amplified from pTagRFP-N1 (Evrogen) by PCR and cloned into the BamHI/EcoRI sites of pcDNA3 to produce pcDNA3-RFP. To generate the expression constructs for the RFP-DCP1A and RFP-EXOSC5 fusion proteins, EcoRI/NotI cDNA fragments of human DCP1A and human EXOSC5 were amplified from a 293T cDNA library by PCR, and cloned into the EcoRI/NotI sites of pcDNA3-RFP to produce pcDNA3-RFP-DCP1A and pCDNA3-RFP-EXOSC5.

Mice, Cells, and Viruses. C57BL/6 mice were purchased from CLEA Japan, Inc. *Irf3*$^{-/-}$*Irf7*$^{-/-}$ mice were kindly donated by T. Taniguchi (The University of Tokyo, Tokyo, Japan). The *Ddx58*$^{-/-}$*Ifih1*$^{-/-}$ mice have been described previously (45). The mice were maintained in our animal facility and treated in accordance with the guidelines of Osaka University. Primary MEFs were prepared from pregnant female mice on embryonic day 13.5, as described previously (4). To prepare bone marrow-derived dendritic cells, mouse bone marrow cells were cultured in the presence of 10 ng/mL GM-CSF (PeproTech) for 6 d, during which time the culture medium was replaced with medium containing GM-CSF every 2 d. The 293T cells have been described previously (46). Replication-competent MLV was produced by 293T cells transfected with pMLV-48. To induce infection, MLV was incubated with MEFs for 2 h in the presence of 10 μg/mL Polybrene (Millipore). VSV, IAV (A/Puerto Rico/8/34, H1N1 strain), and NDV have been described elsewhere (3, 4).

Quantitative RT-PCR. Total RNA was isolated using the ZR RNA MicroPrep kit (Zymo Research), according the manufacturer's instructions. Viral RNA was isolated from the culture supernatants using the ZR Viral RNA kit (Zymo Research), according the manufacturer's instructions. RT was performed using random primers and Verso reverse transcriptase (Thermo Scientific) according to the manufacturer's instructions. For quantitative PCR, the cDNA fragments were amplified from the RT products with Real-Time PCR Master Mix (Toyobo) according to the manufacturer's instructions. The fluorescence from the TaqMan probe for each cytokine was detected with a 7500 Real-Time PCR System (Applied Biosystems). To determine the relative induction of cytokine mRNAs, the level of mRNA expressed from each gene was normalized to the expression of 18S RNA. The copy number of the MLV genomic RNA was determined with the dsDNA copy number calculator program. The experiments were repeated at least three times, with reproducible results.

ELISAs. The levels of IFN-β and Cxcl10 in the culture supernatants were measured with ELISAs in accordance with the manufacturer's instructions. The experiments were repeated at least three times, with reproducible results.

Northern Blotting. Cytoplasmic RNA was extracted using the Cytoplasmic and Nuclear RNA Purification Kit (Norgen) according the manufacturer's instructions. The RNA obtained was separated electrophoretically, transferred to nylon membranes, and hybridized with the indicated probes. An RNA probe was designed to hybridize specifically to the Gag region from nucleotide 1291 to nucleotide 1472 of the MLV transcripts. The experiments were repeated at least three times, with reproducible results.

Immunoblotting. Immunoblotting was performed as described previously (47). The experiments were repeated at least three times, with reproducible results.

Immunostaining Assay. Cells cultured in microscopy chambers (ibidi) were fixed with 3% (wt/vol) paraformaldehyde and then processed for immunostaining as described previously (47). The samples were examined under an LSM 780 confocal laser scanning microscope (Carl Zeiss). The experiments were repeated at least three times, with reproducible results.

Detection of the MLV Transcripts with FISH. The cells were fixed with 4% paraformaldehyde. FISH was performed using the QuantiGene ViewRNA ISH Cell Assay kit (Veritas) according to the manufacturer's instructions. A Cy5-labeled FISH probe was designed to hybridize specifically to the Gag region from nucleotide 607 to nucleotide 1833 of the MLV transcripts. The samples were examined under an LSM780 confocal laser scanning microscope. The experiments were repeated at least three times, with reproducible results.

ACKNOWLEDGMENTS. We thank Drs. H. Fan, D. Trono, H. Miyoshi, and T. Taniguchi for providing invaluable materials and the members of the Laboratory of Host Defenses for their assistance. This work was supported by a Japan Society for the Promotion of Science Grant-in-Aid for Challenging Exploratory Research (to T. Saitoh); the Cabinet Office, Government of Japan, and the Japan Society for the Promotion of Science Funding Program for World-Leading Innovative Research and Development on Science and Technology "FIRST Program" (to S.A.); and National Institutes of Health Grant P01-AI070167 (to S.A.).

1. Kawai T, Akira S (2009) The roles of TLRs, RLRs and NLRs in pathogen recognition. *Int Immunol* 21(4):317–337.
2. Iwasaki A (2012) A virological view of innate immune recognition. *Annu Rev Microbiol* 66:177–196.
3. Yoneyama M, et al. (2004) The RNA helicase RIG-I has an essential function in double-stranded RNA-induced innate antiviral responses. *Nat Immunol* 5(7):730–737.
4. Kato H, et al. (2006) Differential roles of MDA5 and RIG-I helicases in the recognition of RNA viruses. *Nature* 441(7089):101–105.
5. Yoneyama M, et al. (1998) Direct triggering of the type I interferon system by virus infection: Activation of a transcription factor complex containing IRF-3 and CBP/p300. *EMBO J* 17(4):1087–1095.
6. Honda K, et al. (2005) IRF-7 is the master regulator of type-I interferon-dependent immune responses. *Nature* 434(7034):772–777.
7. Alexopoulou L, Holt AC, Medzhitov R, Flavell RA (2001) Recognition of double-stranded RNA and activation of NF-kappaB by Toll-like receptor 3. *Nature* 413(6857): 732–738.
8. Yamamoto M, et al. (2003) Role of adaptor TRIF in the MyD88-independent toll-like receptor signaling pathway. *Science* 301(5633):640–643.
9. Cella M, et al. (1999) Plasmacytoid monocytes migrate to inflamed lymph nodes and produce large amounts of type I interferon. *Nat Med* 5(8):919–923.
10. Diebold SS, Kaisho T, Hemmi H, Akira S, Reis e Sousa C (2004) Innate antiviral responses by means of TLR7-mediated recognition of single-stranded RNA. *Science* 303(5663):1529–1531.
11. Heil F, et al. (2004) Species-specific recognition of single-stranded RNA via toll-like receptor 7 and 8. *Science* 303(5663):1526–1529.
12. Kawai T, et al. (2004) Interferon-alpha induction through Toll-like receptors involves a direct interaction of IRF7 with MyD88 and TRAF6. *Nat Immunol* 5(10):1061–1068.
13. Honda K, et al. (2005) Spatiotemporal regulation of MyD88-IRF-7 signalling for robust type-I interferon induction. *Nature* 434(7036):1035–1040.
14. Ihle JN, Rein A, Mural R (1984) Immunological and virological mechanisms in retrovirus-induced murine leukemogenesis. *Advances in Viral Oncology*, ed Klein G (Raven Press, New York), pp 95–137.
15. Schiff RD, Oliff A (1986) The pathophysiology of murine retrovirus-induced leukemias. *Crit Rev Oncol Hematol* 5(3):257–323.
16. Kane M, et al. (2011) Innate immune sensing of retroviral infection via Toll-like receptor 7 occurs upon viral entry. *Immunity* 35(1):135–145.
17. Everitt AR, et al.; GenISIS Investigators; MOSAIC Investigators (2012) IFITM3 restricts the morbidity and mortality associated with influenza. *Nature* 484(7395):519–523.
18. Fensterl V, et al. (2012) Interferon-induced Ifit2/ISG54 protects mice from lethal VSV neuropathogenesis. *PLoS Pathog* 8(5):e1002712.
19. Goubau D, Deddouche S, Reis E Sousa C (2013) Cytosolic sensing of viruses. *Immunity* 38(5):855–869.
20. Gao G, Guo X, Goff SP (2002) Inhibition of retroviral RNA production by ZAP, a CCCH-type zinc finger protein. *Science* 297(5587):1703–1706.
21. Guo X, Carroll JW, Macdonald MR, Goff SP, Gao G (2004) The zinc finger antiviral protein directly binds to specific viral mRNAs through the CCCH zinc finger motifs. *J Virol* 78(23):12781–12787.
22. Guo X, Ma J, Sun J, Gao G (2007) The zinc-finger antiviral protein recruits the RNA processing exosome to degrade the target mRNA. *Proc Natl Acad Sci USA* 104(1): 151–156.
23. Chen G, Guo X, Lv F, Xu Y, Gao G (2008) p72 DEAD box RNA helicase is required for optimal function of the zinc-finger antiviral protein. *Proc Natl Acad Sci USA* 105(11): 4352–4357.
24. Ye P, Liu S, Zhu Y, Chen G, Gao G (2010) DEXH-Box protein DHX30 is required for optimal function of the zinc-finger antiviral protein. *Protein Cell* 1(10):956–964.
25. Wang X, Lv F, Gao G (2010) Mutagenesis analysis of the zinc-finger antiviral protein. *Retrovirology* 7:19.
26. Reineke LC, Lloyd RE (2013) Diversion of stress granules and P-bodies during viral infection. *Virology* 436(2):255–267.
27. Liu Q, Greimann JC, Lima CD (2006) Reconstitution, activities, and structure of the eukaryotic RNA exosome. *Cell* 127(6):1223–1237.
28. Hayakawa S, et al. (2011) ZAPS is a potent stimulator of signaling mediated by the RNA helicase RIG-I during antiviral responses. *Nat Immunol* 12(1):37–44.
29. Paprotka T, et al. (2011) Recombinant origin of the retrovirus XMRV. *Science* 333(6038):97–101.
30. Yamamoto N, Hinuma Y (1985) Viral aetiology of adult T-cell leukaemia. *J Gen Virol* 66(Pt 8):1641–1660.

31. Haseltine WA (1988) Replication and pathogenesis of the AIDS virus. *J Acquir Immune Defic Syndr* 1(3):217–240.
32. Zhu Y, et al. (2011) Zinc-finger antiviral protein inhibits HIV-1 infection by selectively targeting multiply spliced viral mRNAs for degradation. *Proc Natl Acad Sci USA* 108(38):15834–15839.
33. Müller S, et al. (2007) Inhibition of filovirus replication by the zinc finger antiviral protein. *J Virol* 81(5):2391–2400.
34. Bick MJ, et al. (2003) Expression of the zinc-finger antiviral protein inhibits alphavirus replication. *J Virol* 77(21):11555–11562.
35. Okeoma CM, Lovsin N, Peterlin BM, Ross SR (2007) APOBEC3 inhibits mouse mammary tumour virus replication in vivo. *Nature* 445(7130):927–930.
36. Santiago ML, et al. (2008) Apobec3 encodes Rfv3, a gene influencing neutralizing antibody control of retrovirus infection. *Science* 321(5894):1343–1346.
37. Yu P, et al. (2012) Nucleic acid-sensing Toll-like receptors are essential for the control of endogenous retrovirus viremia and ERV-induced tumors. *Immunity* 37(5):867–879.
38. Chen CY, et al. (2001) AU binding proteins recruit the exosome to degrade ARE-containing mRNAs. *Cell* 107(4):451–464.
39. Hurt JA, et al. (2009) A conserved CCCH-type zinc finger protein regulates mRNA nuclear adenylation and export. *J Cell Biol* 185(2):265–277.
40. Liang J, Song W, Tromp G, Kolattukudy PE, Fu M (2008) Genome-wide survey and expression profiling of CCCH-zinc finger family reveals a functional module in macrophage activation. *PLoS ONE* 3(8):e2880.
41. Lai WS, et al. (1999) Evidence that tristetraprolin binds to AU-rich elements and promotes the deadenylation and destabilization of tumor necrosis factor alpha mRNA. *Mol Cell Biol* 19(6):4311–4323.
42. Yu D, et al. (2007) Roquin represses autoimmunity by limiting inducible T-cell costimulator messenger RNA. *Nature* 450(7167):299–303.
43. Matsushita K, et al. (2009) Zc3h12a is an RNase essential for controlling immune responses by regulating mRNA decay. *Nature* 458(7242):1185–1190.
44. Bacheler L, Fan H (1981) Isolation of recombinant DNA clones carrying complete integrated proviruses of Moloney murine leukemia virus. *J Virol* 37(1):181–190.
45. Kato H, et al. (2008) Length-dependent recognition of double-stranded ribonucleic acids by retinoic acid-inducible gene-I and melanoma differentiation-associated gene 5. *J Exp Med* 205(7):1601–1610.
46. Saitoh Y, et al. (2008) Overexpressed NF-kappaB-inducing kinase contributes to the tumorigenesis of adult T-cell leukemia and Hodgkin Reed-Sternberg cells. *Blood* 111(10):5118–5129.
47. Saitoh T, et al. (2008) Loss of the autophagy protein Atg16L1 enhances endotoxin-induced IL-1beta production. *Nature* 456(7219):264–268.

JVI
Journals.ASM.org

Ifit1 Inhibits Japanese Encephalitis Virus Replication through Binding to 5′ Capped 2′-O Unmethylated RNA

Taishi Kimura,[a,b] Hiroshi Katoh,[d] Hisako Kayama,[a,b,f] Hiroyuki Saiga,[a] Megumi Okuyama,[a] Toru Okamoto,[d] Eiji Umemoto,[a,b,f] Yoshiharu Matsuura,[d] Masahiro Yamamoto,[c,e] Kiyoshi Takeda[a,b,f]

Department of Microbiology and Immunology, Graduate School of Medicine,[a] Laboratory of Mucosal Immunology,[b] and Laboratory of Immunoparasitology,[c] WPI Immunology Frontier Research Center, Osaka University, Osaka, Japan; Department of Molecular Virology[d] and Department of Immunoparasitology,[e] Research Institute for Microbial Diseases, Osaka University, Osaka, Japan; Core Research for Evolutional Science and Technology, Japan Science and Technology Agency, Saitama, Japan[f]

The interferon-inducible protein with tetratricopeptide (IFIT) family proteins inhibit replication of some viruses by recognizing several types of RNAs, including 5′-triphosphate RNA and 5′ capped 2′-O unmethylated mRNA. However, it remains unclear how IFITs inhibit replication of some viruses through recognition of RNA. Here, we analyzed the mechanisms by which Ifit1 exerts antiviral responses. Replication of a Japanese encephalitis virus (JEV) 2′-O methyltransferase (MTase) mutant was markedly enhanced in mouse embryonic fibroblasts and macrophages lacking Ifit1. Ifit1 bound 5′-triphosphate RNA but more preferentially associated with 5′ capped 2′-O unmethylated mRNA. Ifit1 inhibited the translation of mRNA and thereby restricted the replication of JEV mutated in 2′-O MTase. Thus, Ifit1 inhibits replication of MTase-defective JEV by inhibiting mRNA translation through direct binding to mRNA 5′ structures.

mRNA has a 5′ cap structure, in which the N-7 position of the guanosine residue is methylated. The 5′ cap structure is known to be responsible for the stability and efficient translation of mRNA (1, 2). In higher eukaryotes, the first one or two 5′ nucleotides are additionally methylated at the ribose 2′-O position by distinct host nuclear 2′-O methyltransferases (MTases) (3, 4). However, the functional role of 2′-O methylation (2′-O Me) remains poorly understood. Several viruses that replicate in the cytoplasm possess their own mRNA capping machineries (5–10). For positive-stranded flaviviruses, nonstructural protein 3 (NS3) acts as an RNA 5′-triphosphatase and NS5 possesses both N-7 and 2′-O MTase activities (8, 11, 12). Recent studies have revealed that 2′-O methylation of the mRNA 5′ cap in these viruses is important for evasion from the host innate immune responses (13–15). However, the 2′-O MTase activity has been shown to be absent from several paramyxoviruses, such as Newcastle disease virus (NDV) and respiratory syncytial virus (RSV) (16, 17).

Type I interferons (IFNs) induce the expression of a large number of antiviral genes through a Janus kinase/signal transducer and activator of transcription (JAK/STAT) pathway (18, 19). Among the IFN-inducible genes, the IFN-inducible protein with tetratricopeptide (IFIT) genes comprise a large family with three (*Ifit1*, *Ifit2*, and *Ifit3*) and four (*IFIT1*, *IFIT2*, *IFIT3*, and *IFIT5*) members in mice and humans, respectively. The murine and human genes are clustered in loci on chromosomes 19C1 and 10q23, respectively (20). IFIT family proteins reportedly associate with several host proteins to exert various cellular functions (21, 22). For example, human IFIT1/IFIT2 and murine Ifit1/Ifit2 bind to eukaryotic translational initiation factor 3 (eIF3) subunits to inhibit translation (23–26). IFIT1 has been suggested to interact with STING/MITA to negatively regulate IRF3 activation (27), whereas IFIT3 may bind TBK1 to enhance type I IFN production and with JAB1 to inhibit leukemia cell growth (28, 29).

In addition to binding host factors, IFIT proteins have functional effects by interacting directly with products of viruses. Human IFIT1 interacts with the human papillomavirus E1 protein and human IFIT2 interacts with the AU-rich RNA of NDV to exert antiviral effects (30, 31). Direct binding of IFIT proteins to virus RNA has also been demonstrated in several recent studies. IFIT1 and IFIT5 bind to the 5′-triphosphate (5′-PPP) RNA that is present in the genomes of viruses (32, 33). Structural studies of human IFIT2 and human IFIT5 identified an RNA-binding site and defined the structural basis of a complex with 5′-PPP RNA (31, 33). However, these structural studies did not explain how IFIT binds to or restricts virus RNA that has a 5′ cap but lacks methylation at the 2′-O position (13–15). Thus, it remains unclear how IFITs mediate antiviral activities against viruses that have a 5′ cap but lack 2′-O MTase activity.

In this study, we analyzed the mechanisms by which murine Ifit1 exerts the host defense against a flavivirus lacking 2′-O MTase activity. Ifit1 was found to preferentially interact with 5′ capped mRNA without 2′-O methylation and inhibit its translation. Thus, Ifit1 participates in antiviral responses targeting 5′ capped mRNA without 2′-O methylation.

MATERIALS AND METHODS

Mice. All animal experiments were conducted in accordance with the guidelines of the Animal Care and Use Committee of the Graduate School of Medicine, Osaka University. The gene-targeting strategies for generating *Ifit1*-knockout (*Ifit1*$^{-/-}$) mice were described previously (34). The *Ifit1*-targeting vector was designed to replace a 1.8-kb fragment encoding the exon of *Ifit1* with a neomycin resistance gene cassette (Neo). A short arm and a long arm of the homology region from the v6.5 embryonic stem (ES) cell genome were amplified by PCR. A herpes simplex virus (HSV) thymidine kinase (tk) gene was inserted into the 3′ end of the vector. After the *Ifit1*-targeting vector was electroporated into ES cells, G418 and ganciclovir doubly resistant clones were selected and screened by PCR and

Received 2 April 2013 Accepted 26 June 2013
Published ahead of print 3 July 2013
Address correspondence to Kiyoshi Takeda, ktakeda@ongene.med.osaka-u.ac.jp.

doi:10.1128/JVI.00883-13

Southern blot analysis. An ES cell clone correctly targeting *Ifit1* was microinjected into C57BL/6 mouse blastocysts. Chimeric mice were mated with female C57BL/6 mice, and heterozygous F1 progenies were intercrossed to obtain *Ifit1*$^{-/-}$ mice.

Cells. HEK293T cells, Vero cells, and mouse embryonic fibroblasts (MEFs) were maintained in Dulbecco's modified Eagle's medium (Nakalai Tesque) supplemented with 10% fetal bovine serum (JRH Bioscience), 100 U/ml penicillin, and 100 μg/ml streptomycin (Gibco). MEFs were prepared from wild-type (WT) and *Ifit1*$^{-/-}$ day 14.5 embryos and immortalized by introduction of a plasmid encoding the simian virus 40 large T antigen. MEFs stably expressing Ifit1 were established by the previously described method with some modifications (34). In short, full-length cDNA of *Ifit1* was cloned into pMRX-puro (pMRX/*Ifit1*). Retrovirus was produced by introduction of pMRX/*Ifit1* into Plat-E packaging cells (35). MEFs were infected with the retrovirus, cultured in the presence of 1 μg/ml of puromycin (Sigma) for 5 days, and harvested for subsequent studies. To isolate peritoneal macrophages, mice were intraperitoneally injected with 5 ml of 4% thioglycolate medium (Sigma), and peritoneal exudative cells were isolated from the peritoneal cavity at 3 days postinjection. The cells were incubated for 2 h and then washed three times with Hanks' balanced salt solution. The remaining adherent cells were used as peritoneal macrophages in the experiments.

Viruses. Japanese encephalitis virus (JEV) strain AT31 (36) was used for the experiments. An NS5 K61A mutation of JEV was introduced into pMWATG1 (37) by PCR-based mutagenesis with the primers 5′-GCGAGGCTCAGCAGCTCTCCGTTGGCTCG-3′ and 5′-CGAGCCAACGGAGAGCTGCTGAGCCTCGC-3′ (the mutagenesis site is underlined) and verified by DNA sequencing. A recombinant virus, the JEV K61A mutant, was generated from pMWJEATG1/JEV K61A as previously described (36). MEFs or macrophages were infected with JEV at specified multiplicities of infection (MOIs). The virus yields in the culture supernatants were titrated by focus-forming assays on Vero cells and expressed as the number of focus-forming units (FFU), as previously described (38). The virus RNA accumulations in the JEV-infected cells were determined by real-time reverse transcription-PCR (RT-PCR) with primers targeting JEV NS5, normalized to the level of host GAPDH (glyceraldehyde-3-phosphate dehydrogenase), and expressed as the fold change in *Ifit1*$^{-/-}$ cells versus wild-type cells (value for wild type = 1).

Preparation of RNA. The 5′-terminal 200 nucleotides of the JEV genome were amplified by PCR using pMWATG1 (37) with the primers 5′-TAATACGACTCACTATTAGAAGTTTATCT-3′ (the T7 class II promoter sequence is underlined) and 5′-CATTACTACCCTCTTCACTCCCACTAGTGG-3′, and the luciferase reporter gene (*luc2*) was amplified using pGL4.14 (Promega) with the primers 5′-TAATACGACTCACTATAGGCCACCATGGAAGATGCCAAAAA-3′ (the T7 class III promoter sequence is underlined) and 5′-TACCACATTTGTAGAGGTTTTACTTGCTTT-3′. Subsequently, the PCR products were *in vitro* transcribed under the control of the T7 promoter with MEGAScript (Ambion). Biotin-labeled RNA was prepared by *in vitro* transcription in the presence of biotin-labeled UTP (PerkinElmer). Capped RNA substrates were produced with a ScriptCap 7-methylguanosine (m7G) capping system (Epicentre) in the presence (5′ cap positive [5′ cap$^+$]/2′-O Me positive [2′-O Me$^+$]) or absence (5′ cap$^+$/2′-O Me negative [2′-O Me$^-$]) of a ScriptCap vaccinia virus 2′-O MTase (Epicentre). ^{32}P-labeled m7GpppA-RNA substrate was prepared with a ScriptCap m7G capping system in the presence of ^{32}P-labeled GTP. A 5′ OH-RNA substrate was produced by incubating *in vitro*-transcribed RNA with calf intestinal alkaline phosphatase (CIAP) for 3 h at 37°C. All RNA substrates were purified with an RNeasy minikit (Qiagen) and stored at −80°C until use.

Real-time RT-PCR. Total RNA was isolated with the TRIzol reagent (Invitrogen), and 1 to 2 μg of RNA was reverse transcribed using Moloney murine leukemia virus reverse transcriptase (Promega) and random primers (Toyobo) after treatment with RQ1 DNase I (Promega). Real-time RT-PCR was performed in an ABI 7300 apparatus (Applied Biosystems) using a GoTaq real-time PCR system (Promega). All values were normalized by the expression of the GAPDH gene. The following primer sets were used: for the JEV NS5 gene, 5′-AACGCACATTACGCGTCCTAGAGATGA-3′ and 5′-CTAACCCAATACATCTCGTGATTGGAGTT-3′; for *Ifnb*, 5′-GGAGATGACGGAGAAGATGC-3′ and 5′-CCCAGTGCTGGAGAAATTGT-3′; for *luc2*, 5′-CCATTCTACCCACTCGAAGACG-3′ and 5′-CGTAGGTAATGTCCACCTCGA-3′; and for the GAPDH gene, 5′-CCTCGTCCCGTAGACAAAATG-3′ and 5′-TCTCCACTTTGCCACTGCAA-3′.

Recombinant proteins. Wild-type and K61A mutant JEV N-terminal NS5 (MTase domain) cDNAs were obtained by PCR using pMWATG1 with the primers 5′-GGATCCGGAAGGCCTGGGGGCAGGACGCTA-3′ and 5′-CTCGAGATGCTCAGGGTCTTTGTGCCACGT-3′. Full-length murine *Ifit1* cDNA and JEV MTase cDNA were inserted into pET-15b and pGEX-6P, respectively. pET/*Ifit1* and pGEX/JEV MTases were transformed into the *Escherichia coli* BL21(DE3) strain. Expression of the Ifit1 and JEV NS5 proteins was induced by addition of 0.5 mM isopropyl-1-thio-β-D-galactopyranoside (IPTG), and the expressed Ifit1 and JEV MTase proteins were purified using Ni^{2+}-affinity chromatography (Novagen) and glutathione-Sepharose 4B (Amersham Biosciences), respectively, according to each manufacturer's instructions. The purified protein was desalted and concentrated using an Amicon Ultra centrifugal filter unit (Millipore) and stored at −80°C until use.

***In vitro* MTase activity assay.** The MTase reaction was performed in a 20-μl reaction mixture of 50 mM Tris-HCl (pH 8.0), 6 mM KCl, 1.25 mM $MgCl_2$, and 0.5 mM *S*-adenosylmethionine (AdoMet) containing 10 nmol of ^{32}P-labeled m7GpppA-RNA substrate (JEV 5′-terminal 200 nucleotides) and 30 pmol of JEV MTase or 80 units of vaccinia virus 2′-O MTase (Epicentre) for 3 h at 37°C. The RNA was purified by passage through a postreaction cleanup column (Sigma) and digested with 10 U of nuclease P1 (Wako) in 50 mM sodium acetate overnight at 37°C. The samples were analyzed on thin-layer chromatography polyethyleneimine (PEI)-cellulose plates developed with 0.3 M ammonium sulfate.

RNA EMSAs. RNA electrophoretic mobility shift assays (EMSAs) were performed using a LightShift chemiluminescent RNA EMSA kit (Thermo Scientific) according to the manufacturer's instructions. Briefly, 0 to 20 pmol of recombinant murine Ifit1 and 2.5 pmol of *in vitro*-transcribed and biotin-labeled RNA were coincubated for 30 min at room temperature in RNA EMSA binding buffer (10 mM HEPES, pH 7.3, 20 mM KCl, 1 mM $MgCl_2$, 1 mM dithiothreitol, 0.1 μg/μl of yeast tRNA, 2% glycerol). The resulting Ifit1/RNA complexes were electrophoresed in a 7.5% native polyacrylamide gel. The separated RNAs were transferred to a positively charged nylon membrane and cross-linked at 120 mJ/cm^2 and an absorbance of 254 nm. The membrane was incubated with stabilized streptavidin-horseradish peroxidase conjugate (1:300 dilution; a component of the EMSA kit), and the bound stable peroxide was detected with luminol/enhancer solution (another component of the EMSA kit). The gel-shift band intensities were quantified using ImageJ software (National Institutes of Health).

RNA pulldown assay. For RNA pulldown assays, an expression vector for hemagglutinin (HA)-tagged murine full-length Ifit1 was transfected into HEK293T cells using Lipofectamine 2000 (Invitrogen). The *Ifit1*-transfected cells were lysed in RNA-binding buffer (10 mM HEPES, pH 7.3, 500 mM KCl, 1 mM EDTA, 2 mM $MgCl_2$, 0.1% NP-40, 0.1 μg/μl of yeast tRNA (Ambion), 1 U/ml of RNase inhibitor [Toyobo]), and the lysate (200 μg) was coincubated with 25 pmol of biotin-labeled RNA and streptavidin-agarose (Invitrogen) in RNA-binding buffer for 30 min at room temperature. The binding complexes were washed five times with RNA-binding buffer, followed by SDS-PAGE and immunoblotting with an anti-HA probe (F-7) antibody (Santa Cruz Biotechnology). The intensity of the detected Ifit1 band was quantified using ImageJ software (National Institutes of Health).

RNA immunoprecipitation. RNA immunoprecipitation was performed as described previously (38) with slight modifications. MEFs (2×10^5) stably expressing Flag-tagged Ifit1 were infected with JEV at an MOI of 1.0 and cultured for 24 h. The cells were then lysed in 500 μl of RNA

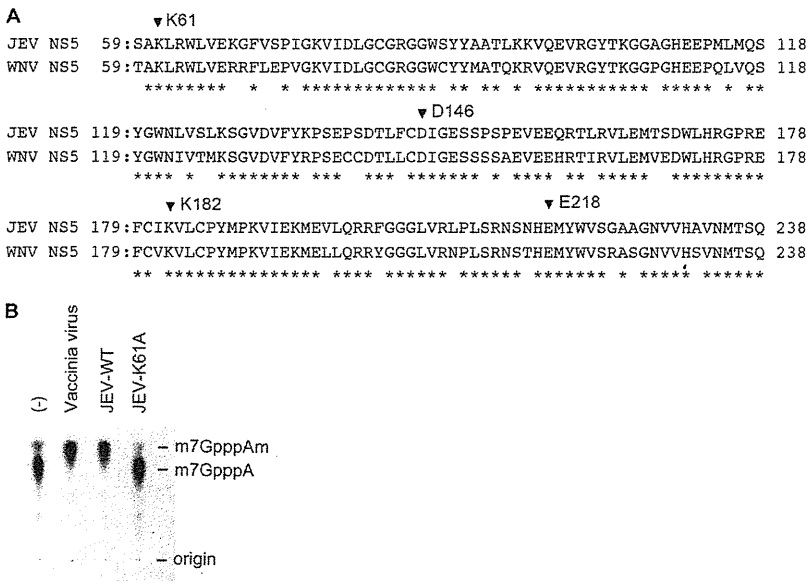

FIG 1 Generation of an MTase-defective JEV mutant. (A) Sequence homology between NS5 proteins of JEV (AT31 strain, GenBank accession number AB196926) and WNV (00-3356 strain, GenBank accession number EF530047). Arrowheads, MTase catalytic K-D-K-E tetrad; *, consensus sequences between the two proteins. (B) 2′-O MTase activity of JEV WT and JEV K61A mutant recombinant NS5 proteins by thin-layer chromatography assays. The substrate m7GpppA-RNA (^{32}P-labeled JEV 5′-terminal 200 nucleotides) was methylated *in vitro* with the respective recombinant NS5 proteins or vaccinia virus 2′-O MTase, digested with P1 nuclease, and developed on PEI-cellulose plates. The positions of 2′-O methylated (m7GpppAm) and unmethylated (m7GpppA) RNA are indicated. Data are representative of four independent experiments.

buffer (10 mM HEPES, pH 7.3, 500 mM KCl, 1 mM EDTA, 2 mM $MgCl_2$, 0.1% NP-40, 0.1 μg/μl of yeast tRNA (Ambion), 1 U/ml of RNase inhibitor [Toyobo], 1 tablet/10 ml of Complete mini-protease inhibitor cocktail [Roche]). After centrifugation at 15,000 rpm for 20 min at 4°C, 50-μl aliquots of the supernatants were recovered as input samples and the remaining supernatants were precleared with 30 μl of 50% protein G-conjugated Sepharose and 1 μg of mouse normal IgG for 1 h. After centrifugation of the beads, the supernatants were immunoprecipitated with 1 μg of mouse normal IgG or anti-Flag M2 antibody (Santa Cruz Biotechnology) and 30 μl of 50% protein G-conjugated Sepharose. The beads were washed five times with RNA buffer without yeast tRNA, and RNA was isolated from the precipitants and input samples with the TRIzol reagent. The RNA was reverse transcribed as described above and subjected to the first round of PCR with JEV NS1-specific primers 5′-TCTG TCACTAGACTGGAGCA-3′ and 5′-CCAGAAACATCACCAGAAGG-3′. The PCR products were then analyzed by quantitative PCR with nested primers 5′-GAGCACTGACGAGTGTGATG-3′ and 5′-AGCGACTCTC AATCCAGTAC-3′. All values were normalized by the values for the input samples (indicated as percent input).

Cellular translational reporter assay. MEFs (2×10^5) were pretreated with 1,000 U/ml of universal type I interferon (PBL Biomedical Laboratories) for 6 h. Three types of 5′ modified luciferase mRNAs (2 μg of 5′-PPP, 5′ cap$^+$/2′-O Me$^-$, and 5′ cap$^+$/2′-O Me$^+$) were transiently transfected into MEFs using the Lipofectamine 2000 reagent (Invitrogen) according to the manufacturer's instructions. At 6 h after the transfection, RNA was isolated and analyzed for the quantity of the luciferase mRNAs (*luc2*). The luciferase activities of whole-cell lysates were measured using a dual-luciferase reporter assay system (Promega). The numbers of relative light units (RLU) were normalized by the concentrations of proteins determined by use of a bicinchoninic acid protein assay kit (Thermo Scientific).

Statistical analysis. Statistical analyses were conducted on each independent data set. An unpaired Student's *t* test was used to determine the statistical significance of differences in the experimental data. *P* values of <0.05 were considered to indicate statistical significance.

RESULTS

***Ifit1*$^{-/-}$ cells fail to restrict the replication of a mutant JEV lacking 2′-O MTase activity.** Previous analysis of the flavivirus West Nile virus (WNV) 2′-O MTase revealed residues in NS5 (K61, D146, K182, and E218) that were essential for its biochemical activity (8). A WNV mutant (E218A) lacking 2′-O MTase activity was attenuated in mouse MEFs and macrophages but showed enhanced replication in *Ifit1*$^{-/-}$ cells (13, 15). As NS5 is a highly conserved protein in flaviviruses, the four residues integral to the 2′-O MTase activity are identical in WNV and JEV (Fig. 1A). Replacement of lysine 61 by alanine in the JEV NS5 MTase domain (JEV K61A) abolished the JEV 2′-O MTase activity *in vitro* (Fig. 1B). We generated *Ifit1*$^{-/-}$ mice (Fig. 2A to C) and infected MEFs with JEV WT and JEV K61A strains (Fig. 3A). The JEV WT replicated equivalently in wild-type and *Ifit1*$^{-/-}$ MEFs. In comparison, the production of the JEV K61A mutant was decreased in wild-type MEFs, suggesting that 2′-O MTase activity is required for JEV replication. Consistent with this and analogous studies with an WNV E218A strain (13), replication of the JEV K61A strain was enhanced (approximately 173-fold increased at 4 days postinfection; $P < 0.05$) in *Ifit1*$^{-/-}$ MEFs compared with wild-type MEFs. We also infected peritoneal macrophages with JEV WT and JEV K61A strains (Fig. 3B). Similar to the results obtained with MEFs, replication of the JEV WT was similarly observed in wild-type and *Ifit1*$^{-/-}$ macrophages. However, replication of the JEV K61A mutant was severely decreased in wild-type but not *Ifit1*$^{-/-}$ macrophages, and the virus was not detected at 4 days postinfection in wild-type cells. For further confirmation, we analyzed virus RNA accumulation at 4 days postinfection (Fig. 3C and D). Whereas RNA levels of JEV WT were similar in wild-type and *Ifit1*$^{-/-}$ MEFs, those of the JEV K61A mutant were markedly

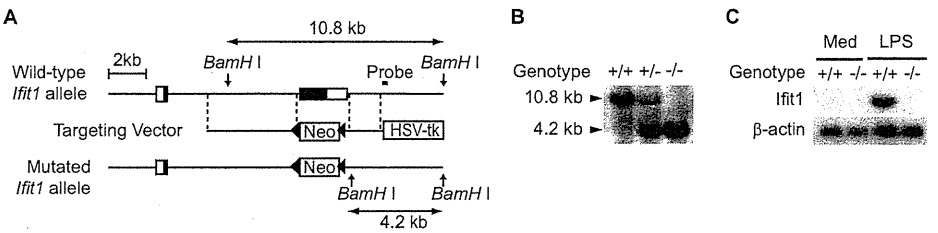

FIG 2 Generation of *Ifit1*$^{-/-}$ mice. (A) Schematic representation of the *Ifit1* gene-targeting strategies. Solid boxes, coding regions of the *Ifit1* gene; open boxes, untranslated regions; Neo and HSV tk, a neomycin-resistance gene cassette and a herpes simplex virus thymidine kinase gene, respectively. The positions of the probe and restriction enzyme site for Southern blotting are shown. (B) Genomic DNA was isolated from the tails of wild-type (+/+), heterozygous (+/-), and homozygous (−/−) *Ifit1* mutant mice. A Southern blot analysis performed after digestion of the genomic DNA with BamHI shows the correct targeting of the locus. (C) Peritoneal exudative macrophages were harvested from wild-type (+/+) or *Ifit1*-deficient (−/−) mice. Total RNA (10 μg) was blotted onto a nylon membrane, and Ifit1 and β-actin mRNA expression was detected by Northern blot analysis with the respective cDNA probes. LPS lanes, cells stimulated with 100 ng/ml of lipopolysaccharide for 4 h to induce endogenous Ifit1 expression; Med lanes, cells treated with medium alone.

higher (approximately 13-fold; $P < 0.05$) in *Ifit1*$^{-/-}$ MEFs than in wild-type MEFs. To further corroborate these findings, we reintroduced the *Ifit1* gene into *Ifit1*$^{-/-}$ MEFs using a retrovirus vector. Replication of the JEV K61A mutant was considerably suppressed (approximately 4-fold; $P < 0.05$) by ectopic Ifit1 expression in *Ifit1*$^{-/-}$ MEFs (Fig. 3E). *Ifnb* was similarly induced in wild-type and *Ifit1*$^{-/-}$ MEFs after infection with the JEV K61A mutant, excluding the possibility that defective type I IFN production is responsible for the high sensitivity to infection with the JEV K61A mutant in *Ifit1*$^{-/-}$ cells (Fig. 3F). Thus, consistent with the findings of previous studies (13, 15), Ifit1 inhibits replication and infection of flavivirus mutants that lack 2′-O MTase activity.

Ifit1 preferentially binds to virus RNA lacking 2′-O methylation. Next, we analyzed how Ifit1 recognizes 2′-O MTase mutant

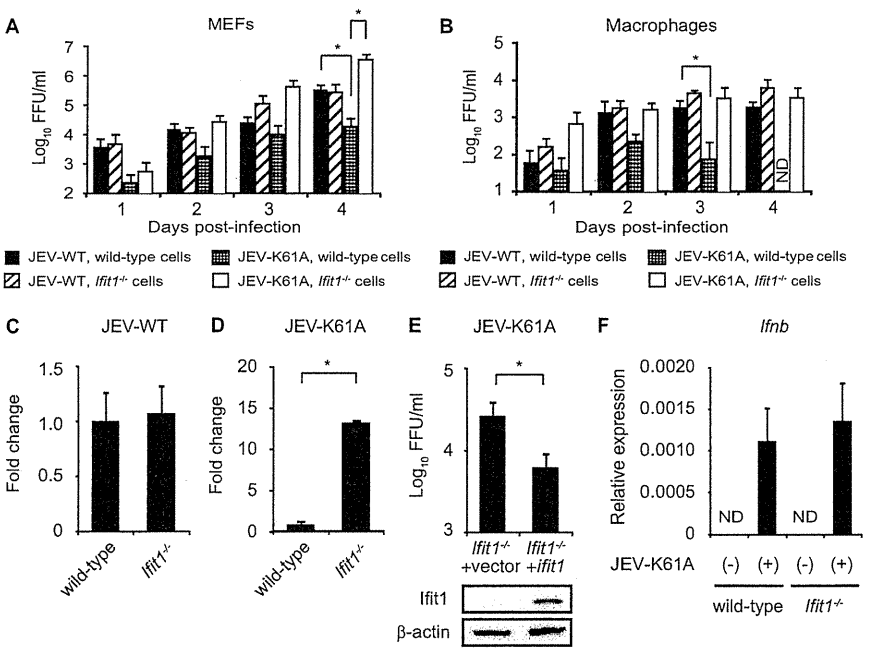

FIG 3 *Ifit1*$^{-/-}$ MEFs and macrophages fail to restrict the replication of the 2′-O MTase mutant JEV. (A, B) Culture supernatants of wild-type and *Ifit1*$^{-/-}$ MEFs (A) and macrophages (B) infected with JEV WT and the JEV K61A mutant (MOIs, 0.1 for MEFs and 0.5 for macrophages) were harvested at the indicated days postinfection. The virus titers in 1-ml supernatant aliquots were determined by focus-forming assays on Vero cells and expressed as the $\log_{10}$ number of FFU/ml. Data are shown as means ± SDs of quadruplicate samples generated from four independent experiments with statistical significance. ND, not detected. *, $P < 0.05$. (C, D) Accumulation of JEV WT (C) and the JEV K61A mutant (D) RNA in wild-type and *Ifit1*$^{-/-}$ MEFs at 4 days postinfection determined by quantitative real-time RT-PCR. JEV NS5 RNA levels were normalized to the level of host GAPDH and are expressed as the fold change in *Ifit1*$^{-/-}$ cells versus wild-type cells (value for wild type = 1). Data are representative of three independent experiments with statistical significance. *, $P < 0.05$. (E) Culture supernatants of vector-transduced (+vector) and Flag-tagged *Ifit1* gene-transduced (+*Ifit1*) *Ifit1*$^{-/-}$ MEFs infected with the JEV K61A mutant (MOI, 0.1) were harvested at 3 days postinfection. The virus titers in 1-ml supernatant aliquots were determined by focus-forming assays on Vero cells and expressed as the $\log_{10}$ number of FFU/ml. Expression of Ifit1 and β-actin determined by immunoblotting with anti-Flag or anti-β-actin antibodies is shown at the bottom. Data are representative of three independent experiments. *, $P < 0.05$. (F) Wild-type and *Ifit1*$^{-/-}$ MEFs were infected with the JEV K61A mutant (MOI, 0.1). At 4 days postinfection, cells were harvested and analyzed for *Ifnb* expression by quantitative RT-PCR. *Ifnb* RNA levels were expressed relative to those of GAPDH. ND, not detected. Data are shown as means ± SDs and are representative of data from three independent experiments.

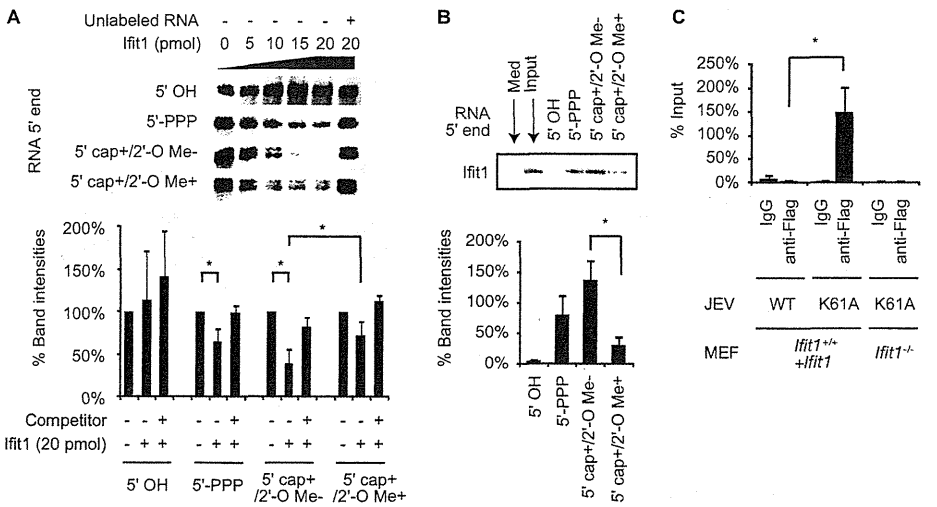

FIG 4 Ifit1 preferentially binds to virus RNA lacking 2′-O methylation. (A) Electrophoretic mobility shift of biotin-labeled RNA (JEV 5′-terminal 200 nucleotides) with recombinant Ifit1. The presence or absence of a 5′ cap and 2′-O Me of the JEV 5′-terminal 200 nucleotides is indicated. Unlabeled 5′-PPP RNA was used as a competitor. The loss of the band indicates binding of RNA and Ifit1 (top). The band intensities (in percent) calculated by ImageJ are shown at the bottom. Data are representative (top) and means ± SDs (bottom) of five independent experiments. *, $P < 0.05$. (B) Lysates from HEK293T cells transfected with HA-tagged Ifit1 were incubated with 2.5 pmol of biotin-labeled RNA. The presence or absence of a 5′ cap and 2′-O Me of the JEV 5′-terminal 200 nucleotides is indicated. 5′ OH RNA was produced by incubating *in vitro*-transcribed RNA with CIAP. RNA was incubated with streptavidin beads, and the precipitates were separated by SDS-PAGE and immunoblotted with an anti-HA antibody (top). Med and Input, samples from whole-cell lysates of empty vector- and *Ifit1*-transfected 293T cells, respectively. The percent band intensities calculated by ImageJ are shown at the bottom. Data are representative (top) and means ± SDs (bottom) of three independent experiments. *, $P < 0.05$. (C) MEFs stably expressing Ifit1 (*Ifit1*$^{+/+}$ + *Ifit1*) or *Ifit1*$^{-/-}$ MEFs were infected with JEV WT or the JEV K61A mutant at an MOI of 1.0. The cells were harvested after 24 h, and JEV RNA/Ifit1-binding complexes were immunoprecipitated with a mouse anti-Flag antibody or mouse IgG. The immunoprecipitated RNA was analyzed by nested RT-PCR using primers that detect the JEV NS1 gene. Each value was normalized by the value for the input (indicated in percent). Data are means ± SDs of three independent experiments. *, $P < 0.05$.

viruses. While recombinant IFIT1 reportedly binds to 5′-PPP RNA (32), the mRNA of the JEV K61A mutant has a 5′ m7G cap but lacks 2′-O methylation (5′ cap$^+$/2′-O Me$^-$). We examined whether Ifit1 can also interact directly with 5′ cap$^+$/2′-O Me$^-$ RNA using electrophoretic mobility shift assays. Consistent with a previous report (32), bands of 5′-PPP RNA but not RNA lacking phosphate at the 5′ end (5′ OH) were diminished after addition of recombinant Ifit1 (Fig. 4A). Furthermore, Ifit1 blocked the electrophoretic mobility of the 5′ cap$^+$/2′-O Me$^-$ RNA. However, this effect was rescued by exogenous addition *in vitro* of 2′-O methylation (5′ cap$^+$/2′-O Me$^+$). The efficient binding of Ifit1 to 5′ cap$^+$/2′-O Me$^-$ RNA was corroborated by RNA pulldown assays (Fig. 4B). HA-tagged Ifit1 was expressed in HEK293T cells, and cell lysates were incubated with biotin-labeled *in vitro*-transcribed RNA and streptavidin-agarose. Then, binding complexes of Ifit1/RNA were analyzed by Western blotting. While Ifit1 was not pulled down with 5′ OH RNA, modest binding of Ifit1 to 5′-PPP RNA and 5′ cap$^+$/2′-O Me$^+$ RNA was observed. In comparison, the strongest Ifit1 protein signal was observed with 5′ cap$^+$/2′-O Me$^-$ RNA. These findings suggest that Ifit1 preferentially binds to 5′ capped RNA lacking 2′-O methylation.

To confirm independently that Ifit1 interacts with 5′ capped RNA lacking 2′-O methylation, we performed RNA immunoprecipitation assays using cell lysates from JEV-infected MEFs that ectopically expressed a Flag-tagged Ifit1. After immunoprecipitation with an anti-Flag antibody, the JEV mRNA was measured by nested RT-PCR analysis (Fig. 4C). JEV RNA was only marginally detected in lysates precipitated with control IgG and lysates of *Ifit1*$^{-/-}$ MEFs infected with the JEV K61A mutant, indicating the specificity of Ifit1 binding in the assay. Virus RNA in JEV K61A mutant-infected MEFs was detected at a level over 37-fold higher than that in JEV WT-infected MEFs. Taken together, these findings suggest that Ifit1 directly interacts with virus mRNA lacking 2′-O methylation.

Ifit1 selectively inhibits translation of 5′ capped 2′-O unmethylated mRNA. To examine the mechanism by which Ifit1 exerts an antiviral effect by associating with mRNA lacking 2′-O methylation, we used a luciferase translational reporter assay. Luciferase RNAs with different 5′ structures were transfected into type I IFN-primed MEFs, and total RNA and cell lysates were harvested 6 h later. Importantly, the levels of luciferase RNAs in wild-type and *Ifit1*$^{-/-}$ cells were unaffected by any of the 5′ modifications (Fig. 5A). We then analyzed the translational efficiency of the transfected RNAs by measuring the luciferase activity (Fig. 5B). As expected (1), uncapped 5′-PPP luciferase mRNA was not translated in either wild-type or *Ifit1*$^{-/-}$ MEFs. Capping of the mRNA (5′ cap$^+$/2′-O Me$^-$) increased translation in wild-type cells, although the levels were profoundly lower ($P < 0.05$) than those in *Ifit1*$^{-/-}$ cells. In comparison, addition of 2′-O methylation to the 5′ cap (5′ cap$^+$/2′-O Me$^+$) *in vitro* resulted in similar levels of translation in wild-type and *Ifit1*$^{-/-}$ MEFs. Even in MEFs that were not treated with type I IFN, similar patterns of luciferase activity were observed (Fig. 5C), indicating that slightly expressed Ifit1 might contribute to the inhibition. Taken together, our data establish that Ifit1 preferentially binds to 5′ capped mRNA lacking 2′-O methylation and inhibits its translation.

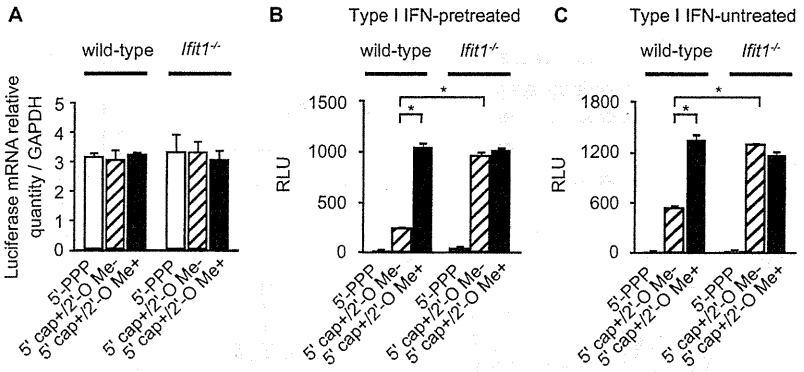

FIG 5 Ifit1 selectively inhibits the translation of mRNA lacking 2′-O methylation. (A) The luciferase RNA amounts at 6 h after RNA transfection were determined by quantitative real-time RT-PCR. The relative luciferase mRNA amounts, calculated as the amount of each transfected mRNA (*luc2*) divided by the level of GAPDH mRNA expression, are shown. The presence or absence of a 5′ cap and 2′-O Me of the introduced luciferase RNA is indicated. Data are shown as means ± SDs and are representative of three independent experiments. (B, C) Wild-type and *Ifit1*$^{-/-}$ MEFs pretreated with type I IFN (B) or untreated (C) were transiently transfected with luciferase mRNA. Luciferase activities were measured at 6 h after the transfection and are shown as relative light units (RLU). The presence or absence of a 5′ cap and 2′-O Me of the introduced luciferase RNA is indicated. Data are shown as means ± SDs of triplicate samples of the representative results. Similar results were obtained in three independent experiments. *, $P < 0.05$.

DISCUSSION

In this study, we investigated the mechanisms by which Ifit1 recognizes RNA of JEV lacking 2′-O MTase activity. Ifit1 inhibited the translation of mRNA through association with mRNA lacking 2′-O methylation.

To analyze the role of Ifit1 in 5′ cap structure-dependent antiviral responses, we generated a JEV MTase mutant. The K61, D146, K182, and E218 residues have all been shown to be essential for the MTase activity of the NS5 protein and replication of WNV (8, 11). While a WNV E218A mutant was previously used for analysis of Ifit1-mediated antiviral responses (13), in our assays, the corresponding JEV E218A mutant was severely impaired in replication in Vero cells and rapidly reverted to the wild type during cell culture, preventing its use (data not shown). A similar phenotype was observed with the WNV D146A 2′-O methylation mutant (11). However, unlike our results, it has recently been reported that a JEV E218A mutant is stable in Vero cells (39). This would be due to the different strains used in the two studies. Thus, mutation of residues that are essential for the 2′-O MTase activity of a flavivirus NS5 protein can differentially impact replication of JEV and WNV even in cells lacking type I IFN responses and IFIT1 expression.

Previous *in vitro* studies indicated that IFIT family proteins bind to several types of RNA, including 5′-PPP RNA and AU-rich double-stranded RNA (31, 32). Indeed, an analysis of the IFIT2 crystal structure indicated the presence of a positively charged RNA-binding channel (31), findings which were supported by the X-ray crystallographic structure of complexes of 5′-PPP RNA with human IFIT5 (33, 40). We also observed that Ifit1 could bind to 5′-PPP RNA. However, our biochemical analysis showed that Ifit1 bound strongly to 5′ capped RNA lacking 2′-O methylation and addition of 2′-O methylation weakened the binding of Ifit1 to the RNA. Since mRNAs of virtually all higher eukaryotes are believed to be methylated at the ribose 2′-O position (41), this modification likely serves as a molecular pattern for discriminating self from nonself.

Although it remains unclear how 2′-O methylation reduces Ifit1 binding to RNA, structural changes to the RNA at the 5′ terminus after 2′-O methylation could sterically hamper Ifit1 binding. The crystal structure of the 5′-PPP RNA/IFIT5 complex has indicated that the RNA-binding site on human IFIT5 is located in a narrow pocket, thus raising the possibility that 5′ capped and 2′-O methylated RNA cannot fit within an analogous pocket of Ifit1 due to a size limitation (33). Future structural analyses of the binding complex of 5′ capped RNA with Ifit1 will be required to reveal the precise mechanisms by which Ifit1 recognizes 5′ capped RNA lacking 2′-O methylation. Additional studies must also test whether other IFITs preferentially associate with 5′ capped RNA lacking 2′-O methylation.

Ifit1 also has an antiviral activity against several negative-stranded viruses, such as vesicular stomatitis virus (VSV) and parainfluenza virus type 5 (PIV5) (32, 42), whose mRNAs are 2′-O methylated (6, 42). In this regard, Ifit1 is supposed to have an antiviral effect independent of 2′-O methylation. Indeed, IFIT1 is able to bind 5′-PPP genomic RNA (32).

Given the previous and present findings that Ifit1 inhibits mRNA translation (23–26), our data are most consistent with a model in which Ifit1 restricts replication of viruses with 5′ capped RNA lacking 2′-O methylation through direct RNA binding and subsequent inhibition of translation. Human IFIT1 and murine Ifit1 were previously reported to interact with eIF3 to interfere with translation (23–26), and replication of hepatitis C virus, whose RNA lacks a 5′ cap, was also impaired by IFIT1 through binding to eIF3 (43). Thus, Ifit1 may associate with both eIF3 and virus mRNA to inhibit translation and infection.

The Ifit family proteins consist of several conserved members. However, Ifit1 and Ifit2 appear to have distinct antiviral activities (44). Thus, the nonredundant and redundant roles of the Ifit family proteins remain to be elucidated. Generation of mice lacking the other members or all of the Ifit family proteins will be useful to reveal the physiological functions.

ACKNOWLEDGMENTS

We thank M. S. Diamond for fruitful discussions and suggestions, T. Wakita for providing us with the JEV AT31 strain, and T. Kitamura for providing us with Plat-E cells. We also thank Y. Magota for technical assistance, C. Hidaka for excellent secretarial assistance, and members of the K. Takeda laboratory for discussions.

This work was supported by grants from the Ministry of Education, Culture, Sports, Science and Technology, the Japan Science and Technology Agency, and The Osaka Foundation for Promotion of Clinical Immunology.

REFERENCES

1. Muthukrishnan S, Both GW, Furuichi Y, Shatkin AJ. 1975. 5′-Terminal 7-methylguanosine in eukaryotic mRNA is required for translation. Nature 255:33–37.
2. Furuichi Y, LaFiandra A, Shatkin AJ. 1977. 5′-Terminal structure and mRNA stability. Nature 266:235–239.
3. Belanger F, Stepinski J, Darzynkiewicz E, Pelletier J. 2010. Characterization of hMTr1, a human Cap1 2′-O-ribose methyltransferase. J. Biol. Chem. 285:33037–33044.
4. Werner M, Purta E, Kaminska KH, Cymerman IA, Campbell DA, Mittra B, Zamudio JR, Sturm NR, Jaworski J, Bujnicki JM. 2011. 2′-O-Ribose methylation of cap2 in human: function and evolution in a horizontally mobile family. Nucleic Acids Res. 39:4756–4768.
5. Both GW, Furuichi Y, Muthukrishnan S, Shatkin AJ. 1975. Ribosome binding to reovirus mRNA in protein synthesis requires 5′ terminal 7-methylguanosine. Cell 6:185–195.
6. Abraham G, Rhodes DP, Banerjee AK. 1975. The 5′ terminal structure of the methylated mRNA synthesized in vitro by vesicular stomatitis virus. Cell 5:51–58.
7. Salas ML, Kuznar J, Vinuela E. 1981. Polyadenylation, methylation, and capping of the RNA synthesized in vitro by African swine fever virus. Virology 113:484–491.
8. Ray D, Shah A, Tilgner M, Guo Y, Zhao Y, Dong H, Deas TS, Zhou Y, Li H, Shi PY. 2006. West Nile virus 5′-cap structure is formed by sequential guanine N-7 and ribose 2′-O methylations by nonstructural protein 5. J. Virol. 80:8362–8370.
9. Decroly E, Imbert I, Coutard B, Bouvet M, Selisko B, Alvarez K, Gorbalenya AE, Snijder EJ, Canard B. 2008. Coronavirus nonstructural protein 16 is a cap-0 binding enzyme possessing (nucleoside-2′O)-methyltransferase activity. J. Virol. 82:8071–8084.
10. Morin B, Coutard B, Lelke M, Ferron F, Kerber R, Jamal S, Frangeul A, Baronti C, Charrel R, de Lamballerie X, Vonrhein C, Lescar J, Bricogne G, Gunther S, Canard B. 2010. The N-terminal domain of the arenavirus L protein is an RNA endonuclease essential in mRNA transcription. PLoS Pathog. 6:e1001038. doi:10.1371/journal.ppat.1001038.
11. Zhou Y, Ray D, Zhao Y, Dong H, Ren S, Li Z, Guo Y, Bernard KA, Shi PY, Li H. 2007. Structure and function of flavivirus NS5 methyltransferase. J. Virol. 81:3891–3903.
12. Dong H, Zhang B, Shi PY. 2008. Flavivirus methyltransferase: a novel antiviral target. Antiviral Res. 80:1–10.
13. Daffis S, Szretter KJ, Schriewer J, Li J, Youn S, Errett J, Lin TY, Schneller S, Zust R, Dong H, Thiel V, Sen GC, Fensterl V, Klimstra WB, Pierson TC, Buller RM, Gale M, Jr, Shi PY, Diamond MS. 2010. 2′-O methylation of the viral mRNA cap evades host restriction by IFIT family members. Nature 468:452–456.
14. Zust R, Cervantes-Barragan L, Habjan M, Maier R, Neuman BW, Ziebuhr J, Szretter KJ, Baker SC, Barchet W, Diamond MS, Siddell SG, Ludewig B, Thiel V. 2011. Ribose 2′-O-methylation provides a molecular signature for the distinction of self and non-self mRNA dependent on the RNA sensor Mda5. Nat. Immunol. 12:137–143.
15. Szretter KJ, Daniels BP, Cho H, Gainey MD, Yokoyama WM, Gale M, Jr, Virgin HW, Klein RS, Sen GC, Diamond MS. 2012. 2′-O methylation of the viral mRNA cap by West Nile virus evades ifit1-dependent and -independent mechanisms of host restriction in vivo. PLoS Pathog. 8:e1002698. doi:10.1371/journal.ppat.1002698.
16. Colonno RJ, Stone HO. 1976. Newcastle disease virus mRNA lacks 2′-O-methylated nucleotides. Nature 261:611–614.
17. Barik S. 1993. The structure of the 5′ terminal cap of the respiratory syncytial virus mRNA. J. Gen. Virol. 74(Pt 3):485–490.
18. Der SD, Zhou A, Williams BR, Silverman RH. 1998. Identification of genes differentially regulated by interferon alpha, beta, or gamma using oligonucleotide arrays. Proc. Natl. Acad. Sci. U. S. A. 95:15623–15628.
19. Takaoka A, Yanai H. 2006. Interferon signalling network in innate defence. Cell. Microbiol. 8:907–922.
20. Fensterl V, Sen GC. 2011. The ISG56/IFIT1 gene family. J. Interferon Cytokine Res. 31:71–78.
21. Sen GC, Fensterl V. 2012. Crystal structure of IFIT2 (ISG54) predicts functional properties of IFITs. Cell Res. 22:1407–1409.
22. Diamond MS, Farzan M. 2013. The broad-spectrum antiviral functions of IFIT and IFITM proteins. Nat. Rev. Immunol. 13:46–57.
23. Hui DJ, Terenzi F, Merrick WC, Sen GC. 2005. Mouse p56 blocks a distinct function of eukaryotic initiation factor 3 in translation initiation. J. Biol. Chem. 280:3433–3440.
24. Terenzi F, Pal S, Sen GC. 2005. Induction and mode of action of the viral stress-inducible murine proteins, P56 and P54. Virology 340:116–124.
25. Terenzi F, Hui DJ, Merrick WC, Sen GC. 2006. Distinct induction patterns and functions of two closely related interferon-inducible human genes, ISG54 and ISG56. J. Biol. Chem. 281:34064–34071.
26. Fensterl V, White CL, Yamashita M, Sen GC. 2008. Novel characteristics of the function and induction of murine p56 family proteins. J. Virol. 82:11045–11053.
27. Li Y, Li C, Xue P, Zhong B, Mao AP, Ran Y, Chen H, Wang YY, Yang F, Shu HB. 2009. ISG56 is a negative-feedback regulator of virus-triggered signaling and cellular antiviral response. Proc. Natl. Acad. Sci. U. S. A. 106:7945–7950.
28. Liu XY, Chen W, Wei B, Shan YF, Wang C. 2011. IFN-induced TPR protein IFIT3 potentiates antiviral signaling by bridging MAVS and TBK1. J. Immunol. 187:2559–2568.
29. Xiao S, Li D, Zhu HQ, Song MG, Pan XR, Jia PM, Peng LL, Dou AX, Chen GQ, Chen SJ, Chen Z, Tong JH. 2006. RIG-G as a key mediator of the antiproliferative activity of interferon-related pathways through enhancing p21 and p27 proteins. Proc. Natl. Acad. Sci. U. S. A. 103:16448–16453.
30. Terenzi F, Saikia P, Sen GC. 2008. Interferon-inducible protein, P56, inhibits HPV DNA replication by binding to the viral protein E1. EMBO J. 27:3311–3321.
31. Yang Z, Liang H, Zhou Q, Li Y, Chen H, Ye W, Chen D, Fleming J, Shu H, Liu Y. 2012. Crystal structure of ISG54 reveals a novel RNA binding structure and potential functional mechanisms. Cell Res. 22:1328–1338.
32. Pichlmair A, Lassnig C, Eberle CA, Gorna MW, Baumann CL, Burkard TR, Burckstummer T, Stefanovic A, Krieger S, Bennett KL, Rulicke T, Weber F, Colinge J, Muller M, Superti-Furga G. 2011. IFIT1 is an antiviral protein that recognizes 5′-triphosphate RNA. Nat. Immunol. 12:624–630.
33. Abbas YM, Pichlmair A, Gorna MW, Superti-Furga G, Nagar B. 2013. Structural basis for viral 5′-PPP-RNA recognition by human IFIT proteins. Nature 494:60–64.
34. Yamamoto M, Okuyama M, Ma JS, Kimura T, Kamiyama N, Saiga H, Ohshima J, Sasai M, Kayama H, Okamoto T, Huang DC, Soldati-Favre D, Horie K, Takeda J, Takeda K. 2012. A cluster of interferon-gamma-inducible p65 GTPases plays a critical role in host defense against Toxoplasma gondii. Immunity 37:302–313.
35. Morita S, Kojima T, Kitamura T. 2000. Plat-E: an efficient and stable system for transient packaging of retroviruses. Gene Ther. 7:1063–1066.
36. Mori Y, Okabayashi T, Yamashita T, Zhao Z, Wakita T, Yasui K, Hasebe F, Tadano M, Konishi E, Moriishi K, Matsuura Y. 2005. Nuclear localization of Japanese encephalitis virus core protein enhances viral replication. J. Virol. 79:3448–3458.
37. Zhao Z, Date T, Li Y, Kato T, Miyamoto M, Yasui K, Wakita T. 2005. Characterization of the E-138 (Glu/Lys) mutation in Japanese encephalitis virus by using a stable, full-length, infectious cDNA clone. J. Gen. Virol. 86:2209–2220.
38. Katoh H, Mori Y, Kambara H, Abe T, Fukuhara T, Morita E, Moriishi K, Kamitani W, Matsuura Y. 2011. Heterogeneous nuclear ribonucleoprotein A2 participates in the replication of Japanese encephalitis virus through an interaction with viral proteins and RNA. J. Virol. 85:10976–10988.
39. Li SH, Dong H, Li XF, Xie X, Zhao H, Deng YQ, Wang XY, Ye Q, Zhu SY, Wang HJ, Zhang B, Leng QB, Zuest R, Qin ED, Qin CF, Shi PY. 2013. Rational design of a flavivirus vaccine by abolishing viral RNA 2′-O methylation. J. Virol. 87:5812–5819.
40. Katibah GE, Lee HJ, Huizar JP, Vogan JM, Alber T, Collins K. 2013. tRNA binding, structure, and localization of the human interferon-induced protein IFIT5. Mol. Cell 49:743–750.
41. Banerjee AK. 1980. 5′-terminal cap structure in eucaryotic messenger ribonucleic acids. Microbiol. Rev. 44:175–205.
42. Andrejeva J, Norsted H, Habjan M, Thiel V, Goodbourn S, Randall RE. 2013. ISG56/IFIT1 is primarily responsible for interferon-induced changes to patterns of parainfluenza virus type 5 transcription and protein synthesis. J. Gen. Virol. 94:59–68.
43. Wang C, Pflugheber J, Sumpter R, Jr, Sodora DL, Hui D, Sen GC, Gale M, Jr. 2003. Alpha interferon induces distinct translational control programs to suppress hepatitis C virus RNA replication. J. Virol. 77:3898–3912.
44. Fensterl V, Wetzel JL, Ramachandran S, Ogino T, Stohlman SA, Bergmann CC, Diamond MS, Virgin HW, Sen GC. 2012. Interferon-induced Ifit2/ISG54 protects mice from lethal VSV neuropathogenesis. PLoS Pathog. 8:e1002712. doi:10.1371/journal.ppat.1002712.

Journal of proteome research

Article

pubs.acs.org/jpr

Understanding the Biological Context of NS5A–Host Interactions in HCV Infection: A Network-Based Approach

Lokesh P. Tripathi,*[,¶,†] Hiroto Kambara,[¶,‡] Yi-An Chen,[†] Yorihiro Nishimura,[‡] Kohji Moriishi,[‡] Toru Okamoto,[‡] Eiji Morita,[‡] Takayuki Abe,[‡] Yoshio Mori,[‡] Yoshiharu Matsuura,[‡] and Kenji Mizuguchi*[,†,§]

[†]National Institute of Biomedical Innovation, 7-6-8 Saito Asagi, Ibaraki, Osaka, 567-0085, Japan

[‡]Department of Molecular Virology, Research Institute for Microbial Diseases, Osaka University, 3-1 Yamada-Oka, Suita, Osaka, 565-0871, Japan

[§]Graduate School of Frontier Biosciences, Osaka University, 1-3 Yamada-Oka, Suita, Osaka, 565-0871, Japan

Supporting Information

ABSTRACT: Hepatitis C virus (HCV) is a major cause of chronic liver disease. HCV NS5A protein plays an important role in HCV infection through its interactions with other HCV proteins and host factors. In an attempt to further our understanding of the biological context of protein interactions between NS5A and host factors in HCV pathogenesis, we generated an extensive physical interaction map between NS5A and cellular factors. By combining a yeast two-hybrid assay with comprehensive literature mining, we built the NS5A interactome composed of 132 human proteins that interact with NS5A. These interactions were integrated into a high-confidence human protein interactome (HPI) with the help of the TargetMine data warehouse system to infer an overall protein interaction map linking NS5A with the components of the host cellular networks. The NS5A–host interactions that were integrated with the HPI were shown to participate in compact and well-connected cellular networks. Functional analysis of the NS5A "infection" network using TargetMine highlighted cellular pathways associated with immune system, cellular signaling, cell adhesion, cellular growth and death among others, which were significantly targeted by NS5A–host interactions. In addition, cellular assays with in vitro HCV cell culture systems identified two ER-localized host proteins RTN1 and RTN3 as novel regulators of HCV propagation. Our analysis builds upon the present understanding of the role of NS5A protein in HCV pathogenesis and provides potential targets for more effective anti-HCV therapeutic intervention.

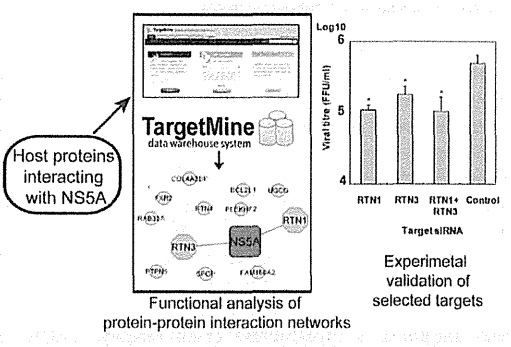

KEYWORDS: *HCV, NS5A, host–pathogen protein–protein interactions, biological network analysis, literature mining, pathway enrichment analysis, siRNA knockdown, target discovery, TargetMine, yeast two-hybrid*

INTRODUCTION

Hepatitis C virus (HCV) causes chronic liver disease including liver steatosis, cirrhosis and hepatocellular carcinoma (HCC) and infects nearly 3% of the world population. HCV possesses a single-stranded RNA genome encoding a 3000 amino acid polyprotein, which is processed by host and viral proteases to yield 10 viral proteins, Core, E1, E2, p7, NS2, NS3, NS4A, NS4B, NS5A and NS5B.[1−5] HCV variants are classified into seven genotypes that display phylogenetic heterogeneity, differences in infectivity and interferon sensitivity.[6,7] However, despite considerable research, a precise understanding of the molecular mechanisms underlying HCV pathology remains elusive.

HCV NS5A protein (hereafter referred to as NS5A) is a RNA binding phosphoprotein, which consists of three domains; domain I includes a zinc-finger motif necessary for HCV replication and an N-terminal membrane anchor region, and the unstructured domains II and III facilitate protein–protein interactions. NS5A plays a critical role in regulating viral replication, production of infectious viral particles, interferon resistance and modulation of apoptosis in HCV pathogenesis via interactions with other HCV proteins and host factors.[8−12] Furthermore, BMS-790052, a small molecule inhibitor of NS5A, is the most potent inhibitor of HCV infection known so far.[13] Consequently, NS5A has emerged as a unique, attractive and promising target for anti-HCV therapy.[14−19] In particular, impairing interactions between NS5A and host factors has been shown to impede HCV infection, which may offer novel anti-HCV therapeutic approaches.[12,20] However, the overall structure and precise functions of NS5A in HCV pathogenesis are poorly understood.

Pathogens such as viruses infect their hosts by interacting with the components of the host cellular networks and

Received: November 30, 2012
Published: May 6, 2013

exploiting the cellular machinery for their survival and propagation. Therefore, elucidating host–pathogen interactions is crucial for a better understanding of pathogenesis.[21−26] Here, we report the host biological processes likely to be influenced by NS5A by virtue of an inferred protein–protein interaction (PPI) network. We describe our integrated approach that combines an experimental yeast two-hybrid (Y2H) assay using NS5A as bait to screen a library of human cDNAs with comprehensive literature mining. The analysis of the NS5A infection network illustrates the functional pathways likely to be influenced by NS5A–host interactions in HCV pathogenesis, thus providing novel insights into the NS5A function in HCV pathogenesis. Furthermore, RTN1 and RTN3, which are endoplasmic reticulum (ER)-localized proteins involved in regulating ER integrity, will be demonstrated as novel regulators of HCV propagation and thus attractive targets for anti-HCV therapy.

MATERIALS AND METHODS

Yeast Two-Hybrid Protein Assay

Screening for the genes encoding host proteins that interact with NS5A was performed using the Matchmaker two-hybrid system (Clontech, Palo Alto, CA, USA) as per the manufacturers' specifications. Human adult liver libraries were purchased from Clontech and were cloned into the pAct2 vector (Clontech) and expressed as fusion proteins fused to the Gal4-activation domain (Gal4-AD). Since Y2H requires the bait protein to translocate to the nucleus, the cDNA of the region corresponding to the NS5A encoding amino acids 1973–2419 (excluding the NS5A N-terminal membrane anchor region) within the HCV polyprotein from the J1 strain (genotype 1b)[27] was amplified by polymerase chain reaction (PCR) and was cloned into the pGBKT7 vector (Clontech)[28] and expressed as Gal4-DNA binding domain (Gal4-DB) fusion in the AH109 yeast strain. The human liver libraries were subsequently screened by Y2H using NS5A as bait. A total of 4×10^6 transformants were screened in this manner, and the positive clones (see Supporting Information) were isolated and sequenced to identify the genes coding for the NS5A interacting host factors (Supporting Information, Table S1).

Literature Mining for Pairwise NS5A–Human Interactions

Literature information describing pairwise interactions between NS5A and cellular proteins were extracted from Medline using the PubMed interface and two other information retrieval and extraction tools, EBIMed[29] and Protein Corral. These tools employ an automatic text-mining approach, but we supplemented them with a follow-up manual inspection. All abstracts related to "NS5A" and "HCV NS5A" keywords and interaction verbs (including "interact", "bind", "attach", "associate")[30] were gathered and manually examined to retrieve direct pairwise NS5A–human protein interactions (see Supporting Information, Tables S2, S3, S4, S5a).

Construction of Extended Protein–Protein Interaction Networks

Physical and direct binary interactions between all human proteins were retrieved from BioGRID 3.1.93[31] and iRefindex 9.0[32] databases using TargetMine.[33] TargetMine is an integrated data warehouse that combines different types of biological data and employs an objective protocol to prioritise candidate genes for further experimental investigation.[33] The interactions were filtered for redundancy, potential false positives and isolated components to infer a representative undirected and singly connected high-confidence human protein interactome (HPI) comprising 22 532 nonredundant binary physical interactions between 7277 proteins (see Supporting Information, Figure S2, Table S5b). The inferred HPI was used to identify biologically relevant trends, the significance of which was assessed by using randomized networks (see below). Secondary interactors of the NS5A interacting proteins were retrieved from the HPI and were appended to the NS5A–host interactions to construct a representative NS5A infection network (Supporting Information, Table S5a).

Topological Analysis

Network components were visualized using Cytoscape,[34,35] while network properties such as *node degree distribution*, *average shortest path* and *betweenness* measures were computed using Cytoscape NetworkAnalyzer plugin[36] as described earlier.[24] For comparison, degree preserved randomized PPI networks were generated by edge rewiring using the Cytoscape RandomNetworks plugin and were used as control networks to assess the statistical significance of the topological trends observed in the inferred PPI networks (see Supporting Information).

Functional Analysis by Characterization of Enriched Biological Associations

Protein structural domain assignments were retrieved from the Gene3D database,[37] Gene ontology associations from the GO consortium,[38] and biological pathway data from KEGG[39] were used to assign functional annotations to the genes in the NS5A infection network. The enrichment of specific biological associations within the NS5A infection network was estimated by performing the hypergeometric test within TargetMine. The inferred p-values were further adjusted for multiple test correction to control the false discovery rate using the Benjamini and Hochberg procedure,[40,41] and the annotations/pathways were considered significant if the adjusted $p \leq 0.005$.

RNAi and Transfection

A mixture of four siRNA targets each to RTN1 and RTN3 (SMARTpool:siGENOME RTN1 siRNA and SMARTpool:siGENOME RTN3 siRNA, respectively) were purchased from Thermo Scientific (Thermo Scientific, Waltham, MA, USA). siGENOME Non-Targeting siRNA Pool #1 (Thermo Scientific) was used as a control siRNA. Thermo Scientific ID numbers of siRNA mixtures of RTN1 and RTN3 and the control were M-014138-00, M-020088-00 and D-001206-13-05, respectively. Each siRNA mixture was introduced into the cell lines by using lipofectamine RNAiMax (Invitrogen, Carlsbad, CA, USA). The replicon cell line, as will be described below, was transfected with each siRNA at a final concentration of 20 nM as per the manufacturer's protocol and then seeded at 2.5×10^4 cells per well of a 24-well plate. The transfected cells were harvested at 72 h post-transfection. The Huh7OK1 cell line, as will be described below, was transfected with each siRNA at a final concentration of 20 nM as per the manufacturer's protocol and then seeded at 2.5×10^4 cells per well of a 24-well plate. The transfected cells were infected with JFH1 at an MOI of 0.05 at 24 h post-transfection. The resulting cells were harvested at the indicated time.

Table 1. List of 132 Human Proteins Interacting with the HCV NS5A Protein

gene ID	symbol	description	refs
47	ACLY	ATP citrate lyase	22
60	ACTB	actin, beta	101
79026	AHNAK	AHNAK nucleoprotein	22
10598	AHSA1	AHA1, activator of heat shock 90 kDa protein ATPase homologue 1 (yeast)	102
207	AKT1	v-akt murine thymoma viral oncogene homologue 1	22
302	ANXA2	annexin A2	103
335	APOA1	apolipoprotein A-I	22
348	APOE	apolipoprotein E	22
116985	ARAP1	ArfGAP with RhoGAP domain, ankyrin repeat and PH domain 1	22
27236	ARFIP1	ADP-ribosylation factor interacting protein 1	22
23204	ARL6IP1	ADP-ribosylation factor-like 6 interacting protein 1	this study
4508	ATP6	ATP synthase F0 subunit 6	this study
8312	AXIN1	axin 1	22
581	BAX	BCL2-associated X protein	22
222389	BEND7	BEN domain containing 7	22
274	BIN1	bridging integrator 1	this study; [22,47]
89927	C16orf45	chromosome 16 open reading frame 45	this study
8618	CADPS	Ca^{++}-dependent secretion activator	22
93664	CADPS2	Ca^{++}-dependent secretion activator 2	22
79080	CCDC86	coiled-coil domain containing 86	22
983	CDK1	cyclin-dependent kinase 1	22
1021	CDK6	cyclin-dependent kinase 6	22
1060	CENPC1	centromere protein C 1	22
153241	CEP120	centrosomal protein 120 kDa	22
11190	CEP250	centrosomal protein 250 kDa	22
9702	CEP57	centrosomal protein 57 kDa	22
80254	CEP63	centrosomal protein 63 kDa	22
1381	CRABP1	cellular retinoic acid binding protein 1	22
1445	CSK	c-src tyrosine kinase	22
1452	CSNK1A1	casein kinase 1, alpha 1	104
1457	CSNK2A1	casein kinase 2, alpha 1 polypeptide	63,105
1499	CTNNB1	catenin (cadherin-associated protein), beta 1, 88 kDa	84,106
9093	DNAJA3	DnaJ (Hsp40) homologue, subfamily A, member 3	22
2202	EFEMP1	EGF containing fibulin-like extracellular matrix protein 1	22
5610	EIF2AK2	eukaryotic translation initiation factor 2-alpha kinase 2	22
2051	EPHB6	EPH receptor B6	this study
54942	FAM206A	family with sequence similarity 206, member A	22
25827	FBXL2	F-box and leucine-rich repeat protein 2	22
2274	FHL2	four and a half LIM domains 2	22
23770	FKBP8	FK506 binding protein 8, 38 kDa	this study; [43,45]
2316	FLNA	filamin A, alpha	12
2495	FTH1	ferritin, heavy polypeptide 1	22
8880	FUBP1	far upstream element (FUSE) binding protein 1	107
2534	FYN	FYN oncogene related to SRC, FGR, YES	22
11345	GABARAPL2	GABA(A) receptor-associated protein-like 2	this study
54826	GIN1	gypsy retrotransposon integrase 1	22
2801	GOLGA2	golgin A2	22
2874	GPS2	G protein pathway suppressor 2	22
2885	GRB2	growth factor receptor-bound protein 2	22
2931	GSK3A	glycogen synthase kinase 3 alpha	22
2932	GSK3B	glycogen synthase kinase 3 beta	22
3055	HCK	hemopoietic cell kinase	22
3320	HSP90AA1	heat shock protein 90 kDa alpha (cytosolic), class A member 1	22
3303	HSPA1A	heat shock 70 kDa protein 1A	108
3315	HSPB1	heat shock 27 kDa protein 1	109
3537	IGLC1	immunoglobulin lambda constant 1 (Mcg marker)	22
79711	IPO4	importin 4	22
3843	IPO5	importin 5	22
3683	ITGAL	integrin, alpha L (antigen CD11A (p180), lymphocyte function-associated antigen 1; alpha polypeptide)	22
6453	ITSN1	intersectin 1	this study
3716	JAK1	Janus kinase 1	22